THE DESIGN AND DEVELOPMENT OF A PHANTOM FOR USE IN DYNAMIC SPECT IMAGING

By

Troy Farncombe

B.Sc., University of Calgary, 1995

A THESIS SUBMITTED IN PARTIAL FULFILLMENT OF

THE REQUIREMENTS FOR THE DEGREE OF

MASTER OF SCIENCE

in

THE FACULTY OF GRADUATE STUDIES

DEPARTMENT OF PHYSICS

We accept this thesis as conforming

to the required standard

THE UNIVERSITY OF BRITISH COLUMBIA

April 1998

In presenting this thesis in partial fulfilment of the requirements for an advanced degree at the University of British Columbia, I agree that the Library shall make it freely available for reference and study. I further agree that permission for extensive copying of this thesis for scholarly purposes may be granted by the head of my department or by his or her representatives. It is understood that copying or publication of this thesis for financial gain shall not be allowed without my written permission.

Department of Physics
The University of British Columbia
6224 Agricultural Road
Vancouver, B.C., Canada
V6T 1Z1

Date: April 24/98

ABSTRACT

It has been suggested that the rate of tracer extraction from certain organs reflects the functional ability of that organ. The determination of the kinetic rates associated with extraction could therefore potentially provide a useful measure of organ function and could help in the diagnosis of disease. Dynamic SPECT is one imaging modality that attempts to determine these kinetic rates in three dimensions.

A dynamic heart-in-thorax phantom has been developed for testing dynamic SPECT reconstruction methods. This phantom consists of a plastic myocardial volume containing smaller "defect" volumes, and a central blood pool. Surrounding the heart phantom is a larger thorax phantom which provides a non-uniform attenuating medium. The heart volumes are loaded with activity and washed out with water, thus producing the same type of activity decay that is seen to occur in the metabolism of fatty acids in the myocardium. By varying the flow rate of water into the phantom, different washout times can be obtained. Additionally, the phantom can be used in a variety of applications including multiple exponential decay and the investigation of input functions.

Testing of the phantom using both planar dynamic and image based SPECT protocols show that the phantom accurately reproduces preset washout rates to within 10%. With this level of accuracy attained, we feel the phantom can confidently be used in the development of new dynamic SPECT reconstruction algorithms.

Table of Contents

List of Figures

List of Tables

ACKNOWLEDGMENTS

I wish to take the time here to thank a few people who have helped me along the way in the preparation of this work. Firstly, my sincere gratitude goes out to my supervisor Anna Celler for allowing me to work with her on this project. Her help and guidance in the work and in the preparation of this thesis has been extraordinary. To her, I say, "dziêkuje bardzo". Also, thank you to Ronald Harrop for all his help and for his helpful critique of the first draft of this work. It's great to get advice from somebody with so much.experience.

Thanks also to Dominik Noll and Jean Maeght in Toulouse, France, for performing some of the reconstructions for me. To Arek Sitek, for helping me with many aspects of SPECT imaging and supplying me with some useful computer code, not to mention enlightening me to the ways of Poland, you are truly a good friend, "dziêkuje". I must also thank the technologists at Vancouver General Hospital for helping with the radionuclide preparation and everyone at the MIRG for being so helpful and friendly.

Lastly, I wish to thank my parents for being so understanding and helping out where they could. This thank you is but a small part of the gratitude to which you are entitled.

CHAPTER 1

INTRODUCTION

Imaging modalities such as x-ray CT, MRI and ultrasound all allow for a non-invasive look into the human body, but with most of these imaging methods, mainly anatomical information is collected. This means that for the most part, any information related to organ function is unavailable. One imaging technique that is inherently functional is nuclear medicine.

In nuclear medicine studies, radiopharmaceuticals are injected into a patient and are designed to be taken up by certain organs and remain stationary in it throughout the time of the study. Single photon emission computed tomography (SPECT) is a nuclear medicine imaging technique that uses a rotating gamma camera in order to acquire projection data of emitted radiation around a patient. This projection data can be reconstructed into a three dimensional map of tracer distribution within the body through the use of a reconstruction algorithm.

It is possible however for some radiopharmaceuticals to be taken up by an organ, metabolized, and then extracted rather quickly. The physiological rates involved in these processes (particularly the extraction), has been shown to be an important indication of organ function [1] [2]. One method that holds potential to determine these washout rates is the technique in nuclear medicine known as dynamic SPECT. The determination

of the kinetic rates is not a trivial task though, as most SPECT cameras are incapable of measuring quick changes in activity distribution in three dimensions due to the acquisition methods currently in use. To overcome this limitation, new algorithms which use a conventional SPECT camera are being developed. Before these new reconstruction techniques can be used clinically, they must first prove themselves in experimental settings.

1.1 Aim of The Work

This work deals with the design and development of a dynamic phantom to be used in the study of different dynamic SPECT reconstruction algorithms. Through testing the phantom under different acquisition protocols and reconstruction methods, a final design has been developed that will be used in the experimental evaluation of such algorithms.

The dynamic phantom described in this thesis is designed to provide experimental radiotracer washout data in three dimensions. This experimental data will be collected with a SPECT camera operating under a variety of different acquisition protocols depending upon the reconstruction algorithm used (see Figure 1.1). Different reconstruction methods will be tested on this data in order to attempt to reconstruct a time activity curve for the region.

1.2 Highlights of the Phantom

The main design objectives have been to produce a phantom that is easy to use, yet provides enough flexibility to allow its use in a variety of studies. Some of the highlights include:

- The size and shape of the dynamic phantom resembles that of a typical human myocardium.

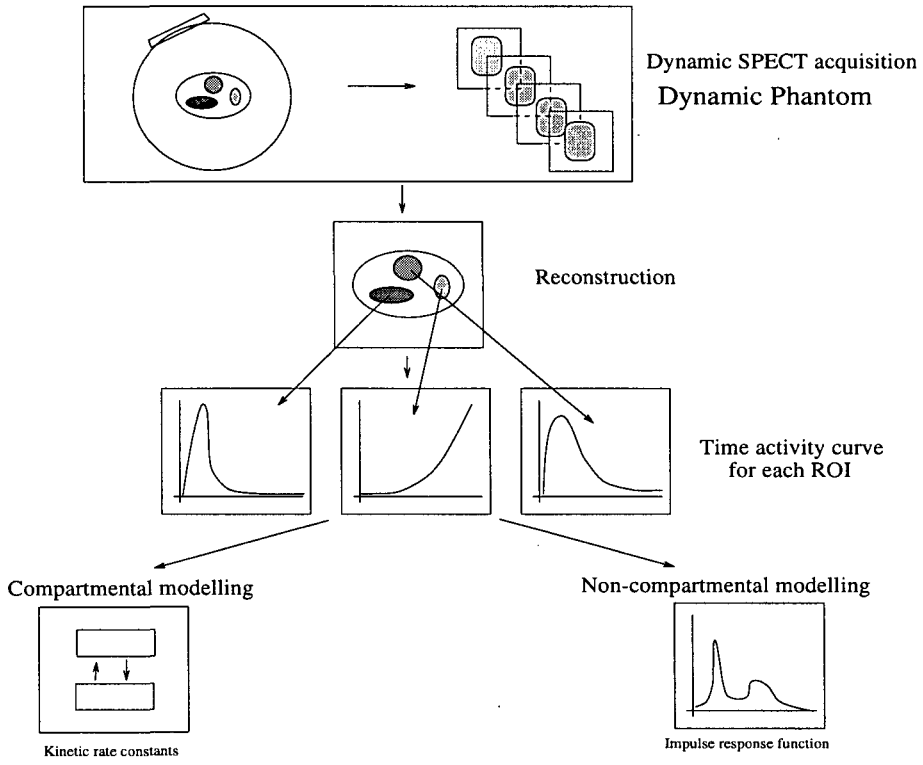

Figure 1.1: The steps used in dynamic SPECT studies. The phantom described will be used to generate experimental washout data to be used in following processes.

- The phantom is designed to model the metabolism of fatty acids in the heart described by a dual exponential function in time. However, the design allows the possibility of modeling between one to ten exponential decays.
- The design allows for up to five different dynamic regions to be imaged simultaneously. While this represents the limit on the apparatus, typically less than five regions will be used at any one time.
- Surrounding the dynamic heart phantom is a model of a human torso. This provides the possibility to test the methods with realistic attenuation conditions.
- The phantom is mobile and so is not camera specific. This allows it to be used with a variety of cameras as well as with other imaging modalities such as PET or MRI.
- Every attempt was made to keep the cost of this phantom low by using commercially

available parts, and doing the manufacturing in house.

1.3 Thesis Organization

This thesis is comprised of seven chapters. Contained within Chapter 2 is information on hardware requirements and image reconstruction techniques used in nuclear medicine. Chapter 3 presents current methods of dynamic imaging and information on dynamic modelling, along with applications.

The design and development of the experimental phantom is divided between Chapter 4 and Chapter 5. The overall design of the phantom is described in these chapters along with results of experiments performed using planar mode. Preliminary tests using dynamic SPECT acquisition are also presented.

Chapter 6 introduces different methods of dynamic SPECT reconstruction and computer simulations that were carried out in order to determine optimal data acquisition protocols.

Finally, Chapter 7 concludes the thesis by presenting other possible applications for the phantom and its future in dynamic SPECT research.

CHAPTER 2

NUCLEAR MEDICINE TECHNIQUES

It is useful in medicine to be able to view inside of a human body through noninvasive techniques. Improved resolution and faster imaging technologies are needed in order for physicians to make more accurate diagnoses.

2.1 MEDICAL IMAGING

Medical imaging was first used clinically soon after Roentgen discovered x-rays over 100 years ago. It was found that when x-rays were incident upon a piece of photographic film, the film would be exposed in these places. It was also noticed that when an object was placed in the path of x-rays, it would attenuate the photons and leave the film less exposed. This fact was exploited in the development of x-ray radiographs and led to the field of medicine known as radiology.

If x-rays passing through a body are then incident upon photographic film, areas of the body containing dense material will absorb more of the photons and leave the film unexposed in these places while areas of soft tissue allow more photons to pass through, thus exposing the film. This imaging technique was seen as a great step forward in diagnostic medicine as for the first time, a physician could see inside a human being

without requiring a scalpel.

As useful as these radiographs were, they were only able to display two dimensional "shadowgrams". In 1973, Hounsfield took x-ray imaging one step further when he developed the first three dimensional method of medical imaging and was able to display cross sectional slices through a living being [3]. His original x-ray scanner had a resolution of about 1 cm^3 and took many minutes to complete a scan across a patient. Through continual developments, today x-ray computed tomography (CT) is able to resolve anatomical details with a resolution on the order of 1 mm^3 and can generate images in less than one second. However, mainly anatomical information is gathered as x-ray CT depends on differences in attenuation coefficients in order to provide information. As attenuation coefficients are dependent upon anatomy, little information can be collected regarding organ function.

Magnetic resonance imaging (MRI) is another imaging modality that uses the magnetic properties of atomic nuclei in order to determine three dimensional images [4]. This modality has resolution comparable to that of x-ray CT, and has shown promise in being able to image organ function through the use of a new technique called functional MRI (fMRI). However, use of fMRI is not common and is not foreseeable in a clinical setting in the near future.

Ultrasound uses high frequency sound waves in order to produce two dimensional images of organ anatomy and motion. Ultrasound images are not of high resolution and have rather poor quality compared to CT or MRI, but it is still very useful even though its information is again, mainly anatomical.

2.2 Nuclear Medicine

Nuclear medicine uses the fact that certain isotopes of elements are unstable. These unstable nuclei decay according to well known Poisson statistics, thereby emitting particles and energy in the form of γ radiation. Most isotopes used in nuclear medicine emit γ rays with energy on the order of several hundred keV. Table 2.1 lists many of the isotopes used in nuclear medicine as well as the photon energies associated with each decay. Note that the positron emitting isotopes (used in PET) are short lived and therefore their use necessitates a cyclotron in close proximity to the imaging centre.

Table 2.1: Common radioactive isotopes used in nuclear medicine.

Isotopes used in single photon imaging.

Isotope	Primary Decay	Photon Energy	Physical Halflife
$^{99m}_{43}Tc$	β^-	140 keV	6.02 hrs
$^{123}_{53}I$	EC	160 keV	13.0 hrs
$^{51}_{24}Cr$	EC	112, 308 keV	23 hrs
$^{131}_{53}I$	β^-	364 keV	8.06 days
$^{133}_{54}Xe$	β^-	80 keV	5.31 days
$^{201}_{81}Tl$	β^-	70, 155, 165 keV	3 days
$^{111}_{49}In$	EC	171, 250 keV	2.83 days
$^{67}_{31}Ga$	EC	93, 185, 300 keV	78 hrs

Positron Emitting Isotopes

Isotope	Primary Decay	Photon Energy	Physical Half-life
$^{11}_{6}C$	β^+	511 keV	20.3 min
$^{13}_{7}N$	β^+	511 keV	10.0 min
$^{15}_{8}O$	β^+	511 keV	2.06 min
$^{18}_{9}F$	β^+	511 keV	109 min

2.2.1 Pharmaceuticals

Nuclear medicine procedures would not be functional if the isotope was always chemically inert in the body. It is important that the isotope, or some compound made with it, takes place in the metabolic processes within the body. The design and manufacture of such compounds is the field known as radiopharmacy.

For the most part, when radioactive isotopes are injected into a body, the distribution of the isotope within the body will be random with no definitive distribution. Certain pharmaceuticals however can be made that localize in specific organs and remain there where they are metabolized. Any compound that tends to target one specific organ of interest is an example of such a pharmaceutical. If these pharmaceuticals can be labelled with a radioactive isotope, they will still localize in the same specific organ, however they will carry the radionuclide with them. By detecting the distribution of the radiopharmaceutical as the radioactive isotope decays, diagnostic information is gathered allowing organ function to be assessed. A list of commonly utilized radiopharmaceuticals in nuclear medicine is shown in Table 2.2.

2.2.2 SPECT Hardware Requirements

In order to detect the presence of a radiopharmaceutical, a NaI scintillating detector is used. A scintillator has the property that when an incoming photon interacts with the crytal, a flash of light is produced. This detector consists of a large (up to 50x50x0.9 cm) NaI crystal coupled to a series of up to 90 photomultiplier tubes [5]. On the face of the NaI crystal is attached a lead collimator as shown in Figure 2.1. This collimator restricts the angle of acceptance of photons into the detector. The most common collimators found on today's cameras are parallel hole collimators which have an acceptance angle of typically $< 3^o$. Other specialized collimators that are also in use are depicted in Figure 2.2.

Table 2.2: Examples of Radiopharmaceuticals used in Nuclear Medicine

SPECT Pharmaceuticals

Compound	Isotope	Application
Sodium Pertechnetate	Tc-99m	Blood flow, tumour determination
Sodium Iodide	I-131	Thyroid function
Xenon gas	Xe-133	Blood flow
IPPA	I-123	Myocardial fatty acid metabolism
DTPA	Tc-99m	Renal glomerular filtration rate
Ortho-Iodo-Hippuran (OIH)	I-131	Renal Studies
Teboroxime	Tc-99m	Myocardial perfusion
DMSA	Tc-99m	Renal morphology
Sestamibi	Tc-99m	Myocardial perfusion

PET Pharmaceuticals

Compound	Isotope	Application
Fluorodeoxyglucose (FDG)	F-18	Tumour and brain metabolism
Ammonia	N-13	Blood perfusion
CO_2	C-11	Blood perfusion
Acetate	C-11	Myocardial metabolism
Water	O-15	Blood flow

On the back of the scintillating crystal there is a series of photomultiplier tubes that are arranged into a close packed array as seen in Figure 2.3.

The outputs from all the photomultiplier are wired together into a summing matrix circuit (SMC) which determines the placement of the detection on the crystal. This circuit consists of a division of the output from each photomultiplier into either an X_i^+ or X_i^- signal and a Y_i^+ or Y_i^- signal and a summation of this divided output into a total X^+, X^-, Y_i^+ and Y^- signal. The output from photomultipliers along the mid line are equally divided into each region. The X,Y position of the photoevent can be determined by using the X^+, X^-, Y_i^+ and Y^- information and the equation,

$$X = \frac{k(X^+ - X^-)}{Z} \quad and \quad Y = \frac{k(Y^+ - Y^-)}{Z} \tag{2.1}$$

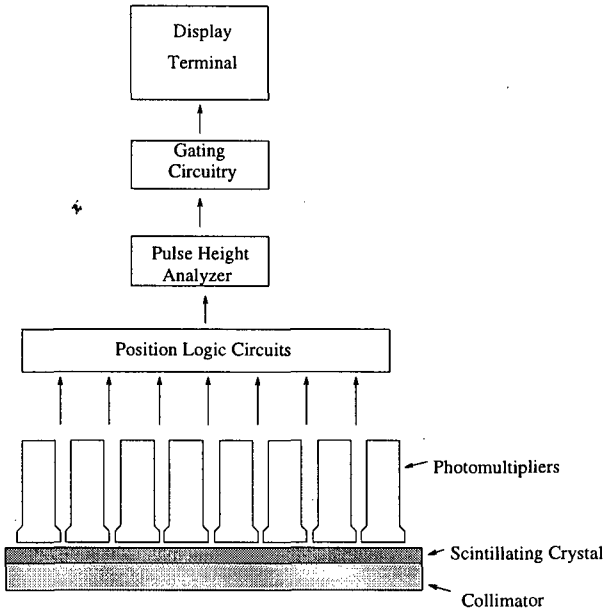

Figure 2.1: A schematic diagram depicting the components of a SPECT camera, from [5].

where Z is the total light output signal and k is a constant. These X and Y values correspond to the position of the detected event in the XY plane. The energy of the decay is determined via a pulse height analyzer. This was the original design of a scintigraphic camera put forth by Harold Anger in 1964 [6].

Using this experimental configuration, a planar image of the radionuclide distribution can be obtained. This planar image is similar to a conventional x-ray radiograph as it consists of an overlapping of all structures within the projection. However, these images are only of limited usefulness as they lack any depth information. In order to reconstruct three dimensional distributions, information needs to be acquired over a range of angles around the object. This technique is known as SPECT (Single Photon Emission Computed Tomography).

In SPECT, planar projections of the activity distribution are measured at a series of angles around the patient. At each angle, acquisition may last up to one minute. The data is collected into typically, a 64x64 or 128x128 pixel array. Typically 64 or 128 projections

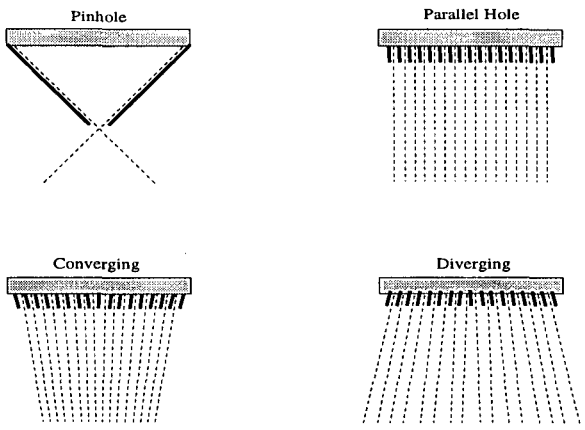

Figure 2.2: Different types of collimators used in nuclear medicine imaging.

are taken over a 180° or 360° angle such that the total scan time of a patient is usually between 20 - 40 minutes. Once projection data has been acquired around the patient, a three dimensional image of the activity distribution is reconstructed.

2.2.3 PET Hardware Requirements

Alternatively to SPECT where only one photon at a time is used for imaging, PET uses positron emitting radioisotopes [7]. A positron travels a very short range ($\approx$ 1-3 mm) before it interacts with an electron in an annihilation. Upon annihiliation, two 511 keV γ photons are released in opposite directions. Because of the short range of the positron, it is assumed that the annihilation occurs in roughly the same position as the nuclide decay. This is an important point as it is the basis of PET imaging.

A PET camera is composed of a circular ring of scintillating detectors surrounding the patient. When a 511keV photon is detected by a particular detector, another photon must be detected in an opposing detector within a small amount of time (called the coincidence window, usually 5-20 ns) in order to be called a coincidence event. If such an event occurs, it indicates that the annihilation occured somewhere along the line connecting

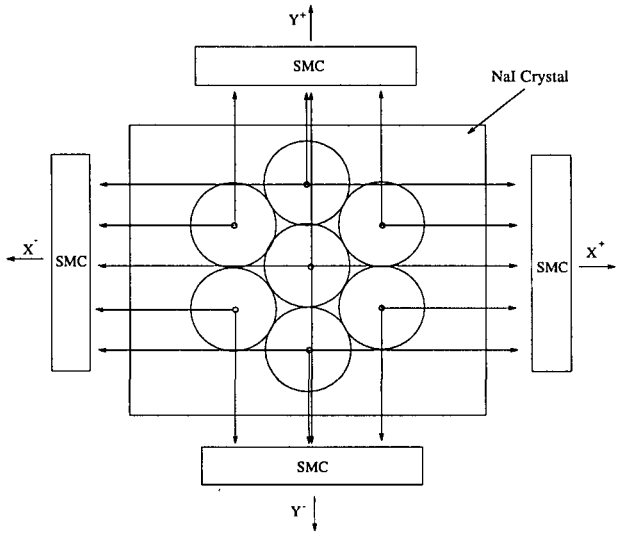

Figure 2.3: The placement of the photomultipliers on the back of the scintillating crystal, from [5].

the two detectors. If no coincidence is detected, the first detected photon is disregarded. Using this type of setup, projection data are obtained and subsequently are reconstructed into a three dimensional activity distribution. A main difference between SPECT and PET is that in PET, all projection data are acquired simultaneously, whereas in SPECT, the camera must perform at least a 180° rotation around the patient in order to collect all projection data necessary for as single image reconstruction.

2.3 Reconstruction Methods

Once projection data is acquired, it can be reconstructed into a three dimensional distribution through the use of various reconstruction algorithms. These algorithms include either analytical methods such as filtered backprojection or Fourier reconstruction, or iterative methods such as maximum likelihood (ML) [8], least squares (LS) or algebraic reconstruction techniques (ART) [9], however, the technique used almost exclusively in commercial nuclear medicine cameras is the filtered backprojection algorithm [10].

The filtered backprojection technique (FBP) uses the projection data acquired by the camera and modifies it through the use of a filter. It then applies a reverse projection (backprojection) to this modified data in order to reconstruct the activity distribution.

The critical requirement in the reconstruction of SPECT images using the conventional reconstruction techniques, is that the radionuclide distribution must remain stationary in the object investigated over the entire scan time. One can imagine however, that as a radiopharmaceutical is metabolized, the distribution of the tracer may change due to the compound being washed out of the organ. When such tracer movement exists, it will be seen in Chapter 3 that it is impossible to determine an accurate representation of the tracer distribution using conventional reconstruction methods.

On the other hand, it has been shown that the metabolic rates associated with various physiological process are important indicators of organ function ability [1, 2]. Therefore, it would be extremely useful to be able to determine these physiological rates in three dimensions in order to gain information related to organ function.

CHAPTER 3

DYNAMIC IMAGING TECHNIQUES

The rate at which physiological processes occur has been found to be a useful measure of the functional ability of an organ [1, 2]. In order to image a dynamic process, an imaging technique must be used that is able to image an object faster than the rate of change in this process. Such a fast image represents a "snapshot" of the process at a given time. If many of these fast images are obtained, then the kinetics of the process can be visualized by viewing all images sequentially in an animation (a cine loop), or this data can be input into various physiological models in order to quantify the physiology.

Alternatively, if information related to the metabolic process is known *a priori*, then this extra information can be used in a dynamic reconstruction method. These two approaches will be discussed in the context of dynamic SPECT in succeeding sections.

3.1 EXISTING DYNAMIC IMAGING METHODS

Currently, four methods are used which satisfy the criteria of fast imaging and hence are able to determine kinetic parameters associated with a metabolic process. These are functional MRI, doppler untrasound, planar nuclear medicine and positron emission

tomography. While these methods work well for some clinical studies, it would be beneficial to develop a three dimensional dynamic imaging method that makes use of common SPECT camera. Possible approaches to dynamic SPECT imaging will be discussed in later sections.

3.1.1 Functional Magnetic Resonance Imaging (fMRI)

Functional MRI is one of the newest imaging modalities available that enables physicians to visualize the functional ability of organs [11, 12, 13]. In functional MRI, very high magnetic field strengths are used in combination with special pulse sequences in order to achieve very fast imaging. With these high speed images, the motion of blood travelling through the body can be imaged and as a result blood perfusion images can be obtained.

3.1.2 Doppler Ultrasound

Ultrasound works by using high frequency sound waves in order to image a two dimensional slice of organ anatomy. By measuring the time elapsed between the emission of an ultrasound wave from a transducer and the subsequent detection of the reflected wave from a boundary, a one dimensional map of the depth of the boundaries can be obtained. If an ultrasonic pulse traverses across a patient, a series of one dimensional mappings is obtained and can be combined into a two dimensional image of organ anatomy.

If the frequency of the reflected ultrasound pulse is measured in addition to the time delay, then a measure of the motion of the reflecting boundary can be done. Because of the Doppler effect, anatomy moving towards the transducer will give rise to an increased frequency in the reflected ultrasound wave, while the reverse motion will lead to a decreased frequency. Usually the motion is viewed on an ultrasound screen by using two different colormaps, red representing motion toward the transducer, and blue representing motion

away from the transducer. This information is useful to measure the relative motion of organs, but such an imaging procedure is not selective to specific processes.

3.1.3 Planar Nuclear Medicine

Planar nuclear medicine dynamic studies are routinely used in clinics in order to gain physiological information. This method is relatively inexpensive, commonly available, and has several clinical applications. After an initial introduction of a radiopharmaceutical into a patient, the pharmaceutical is metabolized and washed out of the targeted organ. If a series of fast planar measurements are taken of the organ during this time, then the uptake and washout will be seen as the tracer concentration within the region changes. In such a study, each image is acquired for only a few seconds while the entire scan may last for several minutes. The result of such a study is a series of images presenting the same region at different times.

Once these planar projections are taken, a region of interest (ROI) is drawn over a specific area of one image and copied on to all succeeding images. The number of counts are obtained in each of these regions and plotted as a function of the time of each image. The result is a time activity curve (TAC) depicting the change in the number of counts in the ROI over time. Once this TAC is drawn, the data is analyzed depending on the information that is required (ie. compartmental model parameters, exponential washout times, etc).

While providing an estimate of the kinetic parameters within an organ, planar dynamic imaging suffers from poor spatial resolution due to the fact that each image is a "shadowgram", much like a conventional x-ray radiograph. Because of this, no information can be obtained regarding the three dimensional distribution of tracer within the organ.

3.1.4 Positron Emission Tomography (PET)

An imaging modality that allows for true three dimensional dynamic imaging is positron emission tomography (PET). PET combines many of the advantages of planar nuclear medicine with the increased spatial resolution of a three dimensional imaging technique.

Because of the fact that a circular array of detectors surrounds the patient, it is possible to obtain data from all projection angles concurrently. This results in high efficiency and fast data acquisition. As data is collected over time, it is divided into a series of data sets, with each set containing projection measurements at all angles collected over a short time interval. Each data set can then be reconstructed using conventional techniques into an image of radiotracer distribution corresponding to a particular moment. By reconstructing a series of data sets, serial images can be obtained with each image representing the tracer distribution at a given time. Once reconstructed, the data is analyzed similarly as in planar nuclear medicine where ROI's are drawn on the images and counts obtained and plotted on a time activity curve. Different modelling techniques are then used to determine the kinetic parameters based upon the pharmaceutical used and the organ in question [14, 15, 16, 17, 18].

Alternatively, kinetic parameters involved in washout may be determined directly from projection data without first going through the time consuming step of reconstructing many images [19, 20]. This method, known as direct parameter reconstruction, has the advantage that all information related to tracer distribution and time is used at once and so does not rely upon the image reconstruction procedure.

As mentioned, dynamic PET offers truly three dimensional imaging capabilities and the ability to determine kinetic parameters of various physiological processes. However, it requires a large capital investment in terms of the PET camera, and a cyclotron to produce isotopes. Therefore very few clinical centers are able to perform such studies, in

fact, of the four PET cameras in Canada, none is used routinely for clinical studies at this time despite their advantages.

3.2 Dynamic SPECT

Dynamic SPECT is a method of dynamic imaging that uses conventional rotating head SPECT cameras in order to determine the kinetic parameters involved in physiological processes. The advantage of using SPECT cameras is that they are widely available, relatively inexpensive, and used in a wide variety of applications.

As mentioned, in order to image dynamic processes, the time needed to complete the scan must be short compared to the time involved for the physiological process. A SPECT camera must rotate at least 180^o around a patient to collect enough data to reconstruct the activity distribution. Since each projection angle takes several seconds in order to collect enough statistical data, a typical SPECT study may take around 30-40 minutes to complete.

Biological half-life is defined as the time required for half of a compound to be removed from an organ. In many important physiological applications, this half-life is on the order of a few minutes, and so conventional SPECT with its slow data acquisition is not able to image these processes properly. In fact, if standard SPECT reconstruction procedures are used to reconstruct tracer washout, severe streaking artifacts will be seen in the reconstructed images [21, 22, 23] and may lead to errors in diagnosis. An example of the streaking artifact is shown in Figure 3.1.

To minimize this artifact, it has been suggested that the data acquisition time not exceed half the biological half-time [21]. If this requirement is met, it has been shown that the resulting streaking artifact in the myocardium will be less than 5% between the lateral wall and septum in healthy tissue [22]. For the kinetics of teboroxime in normally

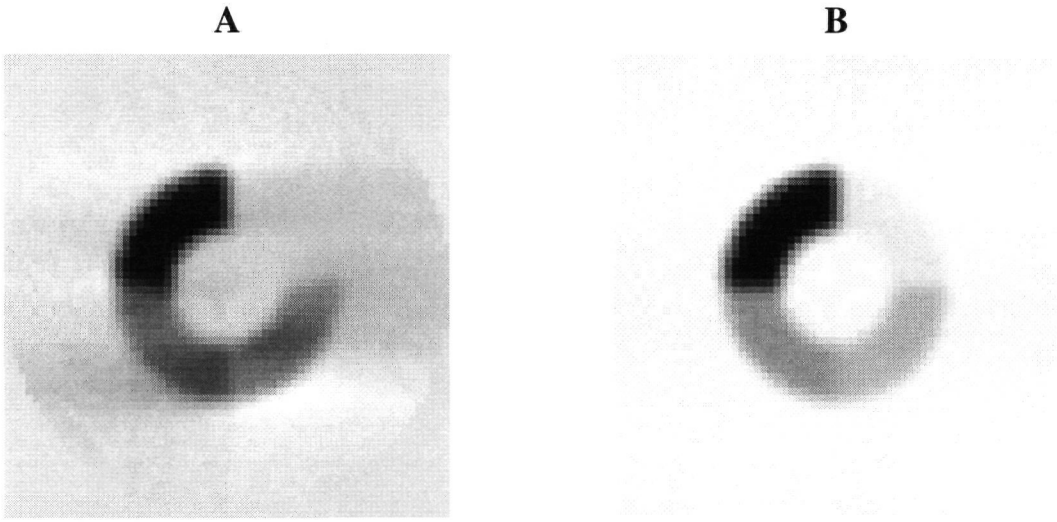

Figure 3.1: A) Streaking artifacts brought about through the reconstruction of dynamically changing data with conventional reconstruction techniques (eg. filtered backprojection). Data was acquired of the phantom shown in B) at time 5 min. Decay times consisted of no decay, 10 min, 5 min and 2 min, proceeding clockwise from the upper left. Data acquisition time was 20 min over 180^o.

perfused myocardium, the biological half time is about 5 min [24]. In order to image such a process with a minimum amount of artifact, the camera will has to rotate a full 180^o in under 2.5 minutes. However, rotating a single headed camera this fast is not a viable solution as not enough data will be collected to be statistically relevant.

One method in which data can be collected in a short amount of time is through the use of high efficiency annular detectors that form a ring around the patient, similar to PET. With this type of ring camera SPECT, projection measurements can be acquired very quickly in order to obtain transverse images every few seconds [25, 26, 27], however such cameras are not commercially available at this time.

Triple head cameras are three times more efficient than single head cameras, and so are able to rotate three times faster around a patient and still collect the same amount of data. For each fast rotation, it is assumed that the tracer distribution remains stationary during

this time and that any tracer movement takes place at the end of the camera rotation. This is a valid assumption provided that the speed of rotation is fast compared to the washout time of the tracer. If this projection data is then reconstructed using conventional reconstruction algorithms, the result will be a transverse image of radiotracer distribution at a certain time, and would appear not unlike a conventional SPECT image.

If another fast rotation is made immediately following the first rotation, and if this data is again reconstructed using conventional reconstruction methods into a transverse image, then this second image will represent the tracer distribution in the same slice, but at a different time. This process can be repeated many times so that a series of images is obtained, with each image representing the tracer distribution at a different time. These reconstructed images are then analyzed by drawing regions of interest (ROI's) and plotting time activity curves in a manner similar to that used for analyzing planar and PET dynamic studies [28]. Such a procedure has already been used in canine cardiac studies [29] and for regional cerebral blood flow (rCBF) [30] with relatively good results. This method is herein referred to as the image based (IB) method as it requires a series of reconstructed images in order to determine the time activity curve. The method is described in further detail in Chapter 6.

Triple head cameras, while becoming more common, are still relatively rare and expensive therefore different methods are currently being developed that hold the promise of using more common, single head SPECT cameras and 180° rotations in order to reconstruct kinetic parameters. These methods use iterative reconstruction algorithms in order to reconstruct kinetic parameters directly from projection data, without first going through the complexity of reconstructing a series of images by using *a priori* knowledge as to the washout of the tracer. Such methods will be referred to as direct parameter (DP) reconstruction methods and will also be described in further detail in Chapter 6.

3.3 Modelling Techniques

The dynamic imaging techniques used in nuclear medicine, including the two methods of dynamic SPECT, attempt to determine the time activity curve for a given region of interest. Regardless of the method used to determine the time activity curve, the data must be fit into a model that represents the internal function of the organ. Such models can never represent the truth of what is actually occuring within the organ, but rather are approximations. Two different approaches which are commonly used to describe the physiology within an organ are the compartmental and non-compartmental models.

3.3.1 Compartmental Modelling

The first modelling technique uses the concept of representing different physiological pathways as compartments. These compartments do not represent physical volumes, but rather volumes in physiological space where each compartment corresponds to a phase in the process of metabolism.

In the simplest one compartment model, the compartment consists of the organ tissue. A radioactive tracer can move freely between the blood and the compartment with the rate of movement in each direction being associated with a kinetic parameter. The rate of change in the amount of tracer present within the compartment, $\frac{dm}{dt}$ can be described by the differential equation,

$$\frac{dm}{dt} = Fc_a - Fc_v \tag{3.1}$$

where m is the mass of tracer present in the compartment, c_a and c_v represent the arterial and venous tracer concentration respectively (equal to $\frac{m}{V}$) and F represents the blood flow rate. In the steady state, the flow rate of tracer out of the compartment must be matched by an equal flow rate of tracer into the compartment, thus resulting in $\frac{dm}{dt} = 0$.

If we now let $j = Fc_a$ and $k = \frac{F}{V}$, equation 3.1 can be rewritten as,

$$\frac{dm}{dt} = j - km \tag{3.2}$$

This equation can be solved for the mass of tracer in the compartment at time T, m(t), by using a Laplace transformation, the solution of which is equal to,

$$m(T) = j * e^{-kt} = e^{-kt}\left\{m(0) + \int_0^T je^{kt}dt\right\} \tag{3.3}$$

As can be seen, if j=0, the solution is simply an exponential washout of tracer in time with a biological half-life given in terms of the decay parameter, k, as,

$$T_{1/2} = \frac{ln(2)}{k} \tag{3.4}$$

A single compartment model does not accurately reflect the physiology occuring within an organ so it is more common to use two or three compartments. Such models however get rather complicated and are beyond the scope of this paper.

3.3.2 Non-compartmental Modelling

For some physiological processes, compartmental analysis fails to accurately determine the kinetic rates involved. In such cases, another technique called non-compartmental modelling is used. Instead of the transportation of tracer being described by differential equations, this method uses transport theory and general signal processing to derive quantitative results from dynamic data.

When a radiopharmaceutical is injected into a patient, the injection should ideally be given as a infinitesimally small bolus described mathematically by a delta function. Over time, as this radiopharmaceutical travels through the body, it is diluted in the blood and taken up by various organs, thereby changing it's concentration. On every pass through

the body, more tracer will be taken up by the organs and removed from the blood. The change of this arterial tracer concentration over time is called the input function. This input function is often determined by a rapid sampling of the arterial blood supply during the course of the study.

The way an organ deals with a pharmaceutical over time is described by the impulse response function. This impulse response function is unique for each organ and is a useful representation of the organ's functional ability. In nuclear medicine imaging, the result of a convolution of the input function with the impulse response function is a time activity curve which represents the amount of tracer within the organ as a function of time. The time activity curve can be written as,

$$y = X * f \tag{3.5}$$

where y and f represent the time activity curve and the impulse response function respectively, and X is the input function. An example of this analysis is shown graphically in Figure 3.3.2.

3.4 Dynamic Applications

As mentioned previously, the determination of physiological rates can be important for diagnosis. Processes such as myocardial fatty acid metabolism, cerebral and renal blood flow and cerebral glucose metabolism are all examples of dynamic processes which have been found to be useful measures of organ function [30, 31]. Their analysis will be discussed in the next section.

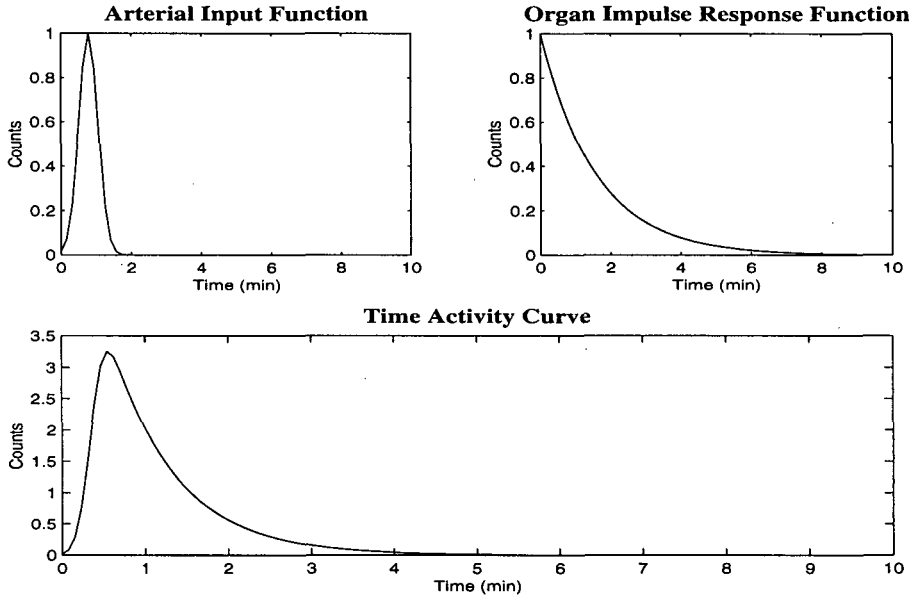

Figure 3.2: An example of a non-compartmental analysis technique showing the input function, impulse response function and the convolution product, the time activity curve.

3.4.1 Compartmental Applications

Some physiological functions have been seen to consist of only a few well known processes within the organ. These functions can be modelled using the compartmental techniques mentioned previously.

The extraction of the cardiac imaging agent Teboroxime, has been described in terms of a one compartment model. The differential equation that describes the tracer flow was given by Equation 3.3. In the metabolism of fluorodeoxyglucose (a glucose analog), a two compartment model is used based on the Sokoloff model with four kinetic rates. For fatty acid metabolism within the myocardium, a three compartment model is used with six kinetic parameters [32].

3.4.2 Non-compartmental Applications

Some of the cases in which compartmental modelling fails to provide an accurate approach are the case of cardiac shunting, certain renal processes, heptabiliary studies and thyroid studies. In these cases, either too many processes are occuring concurrently so that they are difficult to model using compartmental methods, or not enough is known about the internal processes present within the organ. Therefore, non-compartmental methods are used instead.

Consider the case of cardiac shunting between the left and right ventricles. When a tracer is injected into a peripheral vein, it passes through the right atrium, right ventricle and on to the lungs. It then returns to the heart via the pulmonary veins and into the left atrium and left ventricle.

Because of shunting in the left ventricle as a result of an atrial septal defect or a ventricular septal defect, a significant amount of tracer takes a short way back to the heart through the pulmonary artery and veins. It is useful to be able to determine the amount of shunting that is taking place in order to plan further treatment and such a measurement can be obtained using non-compartmental modelling.

Another application of non-compartmental modelling includes certain renal functions. The determination of an impulse response function for the kidneys allows for the investigation of various functional parameters such as perfusion, tracer extraction, and parenchymal transit which can help distinguish between normal and abnormal renal function. Organs such as the liver and thyroid, along with processes such as regional cerebral blood flow are also commonly studied using non-compartmental modelling techniques.

Chapter 4

Myocardial Phantom Principles

4.1 Phantoms

Before any new reconstruction method can be applied clinically, it must be thoroughly tested in order to ensure accurate results. The first way to test a new method of reconstruction is to model experimental data using a computer. This involves either the use of perfect analytical data, or simulations based on statistical models.

These simulations are typically performed in nuclear medicine using Monte Carlo techniques in which the probability of photon interaction in matter is randomly generated for a photon with certain parameters. By altering the parameters of the simulation, different experimental conditions can be modelled. By following the paths of millions of photons, the net distribution of photons is governed by the laws of probability. However, these simulations are very time consuming and often still do not come close enough to actual experimental data to classify them as realistic, and so another way to test the methods must be used that better models a realistic situation.

In order to maintain control of experiments, we make use of yet another tool, a phantom. Phantoms can be based on real anatomy (such as a heart or brain), or they can be simple geometrical objects. It is important, however, that the characteristics of

the phantom are known before any experiment is performed as it makes verification of experimental results easy.

To better describe an idea of a phantom, consider the Jaszczak phantom used routinely in nuclear medicine. This phantom consists of a large cylinder that is filled with water, thus providing tissue-like attenuation. Into this cylinder are placed a series of progressively smaller spheres that are filled with activity. Projection data acquired with this phantom can be reconstructed using various reconstruction techniques. Without knowing the geometry of the phantom beforehand, it may be difficult to decide which reconstruction technique works best. However, it is easier to see which reconstruction methods work better if we already know the phantom geometry and the amount of activity contained within the phantom.

In order to test a method of dynamic SPECT, we must use a phantom that behaves similarly to the physiological process being studied. In this case, we use a dynamic phantom where the amount of tracer contained within the phantom varies in time. We achieve this experimentally by the method described in the following section.

4.2 Principle of the Dynamic Phantom

When a radioactive tracer of activity A, is contained in a volume V, the concentration of the tracer is found by,

$$Concentration(Bq/ml) = \frac{Activity}{Volume} \tag{4.1}$$

If a liquid containing tracer with a different concentration is passed through the volume, the rate of change in the amount of tracer in the volume is equal to the rate of the tracer entering minus the rate of tracer exiting. This equation can be described mathematically by a first order, linear differential equation. This equation is,

$$\frac{dA}{dt} = (CF)_{in} - (CF)_{out} \tag{4.2}$$

where A is the amount of tracer present (Bq), C_{in} = incoming concentration (Bq/ml), C_{out} = outflowing concentration (Bq/ml), and F is the respective water flow rate into and out of the volume measured in (ml/s). For a constant volume, the inflowing liquid rate must be the same as the outflowing liquid rate. Thus, we may write,

$$\frac{dm}{dt} = (C_{in} - C_{out})F \tag{4.3}$$

As $C_{out} = \frac{m(Bq)}{V(ml)}$, then we rewrite 4.3 as,

$$\frac{dm}{dt} = FC_{in} - F\frac{m}{V} \tag{4.4}$$

If we now let $k(s^{-1}) = \frac{F}{V}$ and $j(Bq/s) = FC_{in} = kVC_{in}$, then we have an equation of the form,

$$\frac{dm}{dt} = j - km \tag{4.5}$$

The solution to this equation can best be found through a Laplace Transform such that,

$$p\mathcal{L}(m) = \mathcal{L}(j) - k\mathcal{L}(m) \tag{4.6}$$

which is solved for $\mathcal{L}$. Upon performing this we get,

$$\mathcal{L}(m) = \mathcal{L}(j)\frac{1}{p+k} \tag{4.7}$$

The solution to equation 4.7 is found through a convolution integral so that the amount of material present at time T,

$$m(T) = j * e^{-kt} = e^{-kT}\left[m(0) + \int_0^T je^{kt}dt\right] \tag{4.8}$$

If the volume is simply diluted with pure water, that is, the incoming activity concentration, j, equals 0 Bq/ml, notice that equation 4.8 reduces to a simple exponential decay of activity over time with the decay parameter given as k. By adjusting the flow rate, F (ml/s), and the volume, V (ml), into which the water is injected, different washout rates, k (s^-1), can be obtained. The combination of different washout rates with different acquisition protocols allows for a wide variety of experimental configurations.

4.2.1 Myocardial Fatty Acid Metabolism

The heart has a natural affinity for the metabolism of fatty acids. These fatty acids consist of long chains of organic molecules. When fatty acids are present in the bloodstream, they are taken up by the heart and enter into one of two compartments, the cellular mitochondria, or into a reserve of triglycerides. In the triglyceride pool, the acids are stored and are metabolized slowly over time. In the cellular mitochondria however, metabolism occurs quickly in a process known as β-oxidation.

In β-oxidation, fatty acids are broken down into smaller molecules, thereby supplying energy to the heart and creating CO_2 as a product. The process of metabolism cannot be seen directly as no distinguishing characteristics are present. However, if a fatty acid is attached to I^{123} labelled benzoic acid [33], thereby creating iodophenylpentadecanoic acid (IPPA), the fatty acid will still take part in β oxidation, but the iodobenzoic acid will be left over as a byproduct when the metabolism ceases [34]. The iodobenzoic acid molecule will then be washed out of the cell and pass through the kidneys into the urine, to be excreted. It has been suggested [35, 36] that the rate at which the benzoic molecule is washed out of the myocardial cell is a good measure of the rate at which β-oxidation is

occuring. Under ischemic conditions, the oxidation of fatty acids will be slower and hence lead to a decrease in the washout of iodobenzoic acid. Therefore, if the rate of extraction of iodobenzoic acid from the heart can be found, then information can be had regarding myocardial viability.

It has been shown that the efficacy of benzoic acid within the myocardium can be described by a dual exponential function as shown in equation 4.9 where λ and η correspond to the rates bezoic acid washout from the β oxidation and triglyceride metabolism respectively.

$$A(t) = A_0 e^{-\lambda t} + B_0 e^{-\eta t} + C_0 \tag{4.9}$$

The washout half lives involved are typically about 10-15 min for λ and around 60-100 min for η [31]. When short acquisition time scales are involved, the efficacy of fatty acids can be approximated by the single exponential decay involving only the fast component.

4.3 Myocardial Phantom

We have designed and built a phantom that models the metabolism of the fatty acid tracer IPPA within the myocardium by using this dilution principle [37]. The design of this phantom consisted of a two small "defect" volumes contained within a larger heart volume. Experimentally, the containers would be loaded with activity and washed out with pure water, thus resulting in an exponential decrease in the amount of activity present over time. The defect volumes would act as regions exhibiting different washout times and hence would correspond physiologically to areas of the myocardium with decreased oxygenation (ischemic). The larger heart container would be filled with activity and washed out at a constant rate typical of that found clinically.

Surrounding the heart container is a model of a human torso. This external part

consists of a large cylinder into which the heart phantom resides. Its volume is 22 liters and may be filled with water in order to provide an attenuating medium. As well, an aluminum spinal column and two celluloid lung objects are present in the thorax in order to create a more realistic phantom with non-uniform attenuation.

Chapter 5

Development of the Myocardial Phantom

The testing of the phantom consisted of two phases. Phase I involved planar testing of the phantom performance in order to verify that the preset washout times corresponded to those actually seen. In phase II, dynamic SPECT protocols were used in order to test the phantom in three dimensions and to provide preliminary experimental data for the evaluation of different dynamic SPECT methods. Based on estimates of clinical data, it was decided that an accuracy of $< 10\%$ between experimental and preset washout rates would be required in phase I before proceeding to phase II.

5.1 Data Acquisition and Analysis

In order to verify the phantom performance prior to dynamic SPECT studies, dynamic planar tests were performed. The defect containers were filled with activity and diluted the with pure water at a preset washin rate, thereby following the equation described in Equation 4.8. Data would be collected by a SPECT camera operating in dynamic planar mode. This acquisition protocol consisted of collecting a series of images of the phantom

every few seconds. It was decided that the best acquisition protocol would be planar images taken in intervals of no longer than 10% of the desired washout time and over a minimum of two half-lives. So, for a preset washout time of 300 s, the acquisition would take place in no longer than 30 s intervals over at least 600 s total, yielding 20 images in total.

The planar data was then analyzed on a workstation consisting of an Apple PowerMac 9500 running Siemens ICON software. A analysis program was written in the Macro Programming Environment (MPE), that enabled us to analyze the data acquired on any SPECT camera within the department. This program allowed us to perform the following.

1) Select the images in the data set to be used to draw the time activity curve.

2) Sum together the selected images into a better defined image in order to differentiate areas of interest.

3) Draw a region of interest (ROI) on this summed image.

4) Copy this ROI to all images and obtain the number of counts contained for each image within this ROI.

5) Create a time activity curve using this information.

6) Fit data to the required function (exponential decay) and display the results.

Once the data acquisition protocol and analysis was established, the next step was to verify the performance of the phantom.

5.2 Calibration

Initially the myocardial phantom consisted of only two dynamic defect containers and a larger dynamic heart volume. The infusion of water into the phantom was controlled via a gravity flow with water rates preset using flowmeters.

These flowmeters consisted of a small diameter glass tube inside of which was a glass marble. The flowmeter was placed in a vertical position with the incoming fluid entering through a bottom inlet and exiting through an upper outlet. On the bottom of the flowmeter was a small graduated dial that adjusts the flow rate of the liquid passing through the meter.

In total, three different flowmeters were used for the experiments: two low flow rate (0-15 ml/min) meters and one medium flow rate (0-50 ml/min) meter. The low rate flowmeters were used with the smaller volume defect containers while the medium rate flowmeter was used with the larger heart container.

Supplied with the flowmeters from the manufacturer was a table of flowmeter settings as marked on the graduated dial versus the actual rate of flow calibrated in ml/min. Such a table had to be checked for accuracy and consistency, so our first experiment was the calibration of the flowmeters. The accuracy of the flowmeters was 5% as stated by the manufacturer.

A simple, yet effective calibration of the flowmeters was performed by measuring the volume of water passing through the flowmeter in a set amount of time for a specific setting on the flowmeter dial. For consistency, all readings were taken from the top of the glass marble. A linear plot of flow rate vs flowmeter setting was then made for the calibration. Calibration curves for each of the three flowmeters are shown in Figure 5.1.

Upon calibrating the flowmeters for the appropriate flow rates, we then commenced dynamic planar trials using one dynamic container at a time, with no thorax attenuation.

5.3 Trial 1: Flowmeters

Initially, only a single container was used. The inlet into the dynamic container consisted of a short length of neoprene tubing and at the end of this tubing was a large hole. The

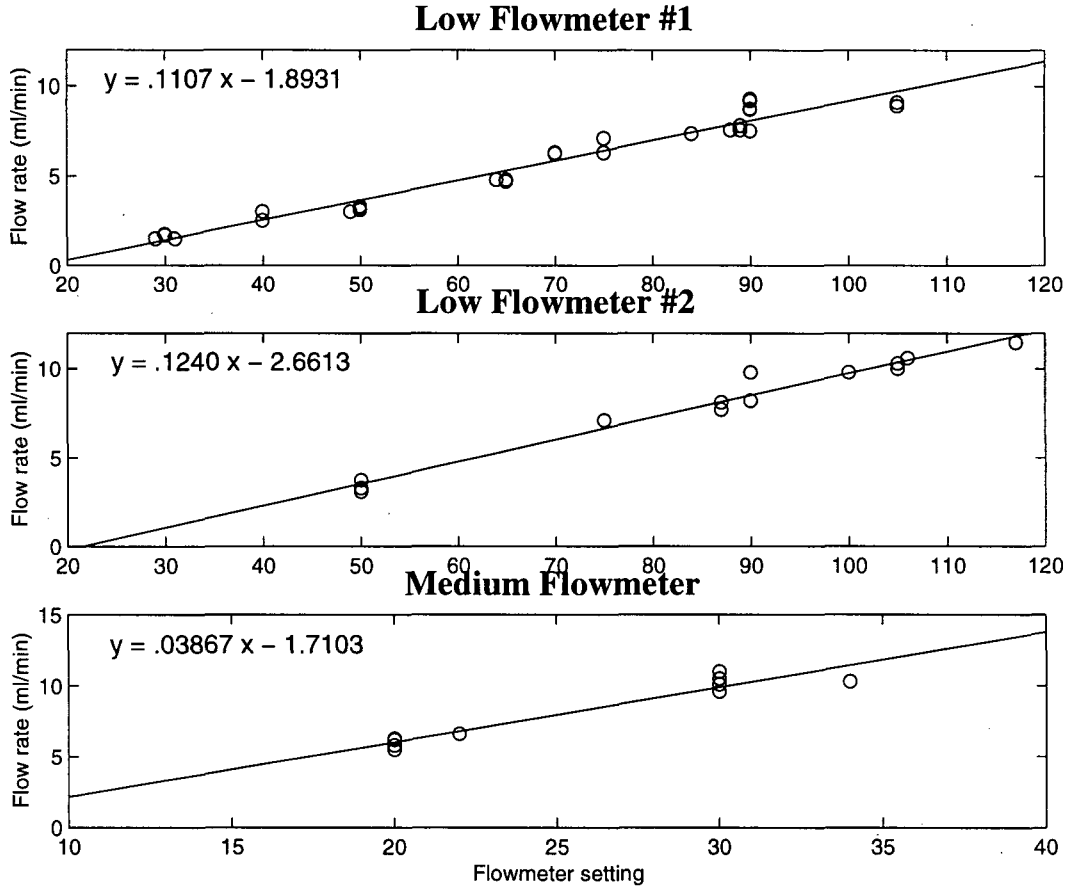

Figure 5.1: Calibration curves for the three flowmeters.

outlet was simply a piece of tubing cut flush with the top of the defect container. A coloring agent was added to the water in the container in order to visually see how the water was mixing with the radioactivity.

Experiments were performed on a Sopha DST dual head camera acquiring in planar dynamic mode with only one head recording counts. Initial activity injected into the phantom was 2 mCi and washout times preset with the flowmeters ranged from 60 - 300 s. Data was acquired into a 64x64 matrix with a time per frame ranging from 5 - 10 s. Experimental configurations are shown in Table 5.1.

Table 5.1: Initial experiments using gravity flowmeters.

	Bottle A	Bottle B	Bottle C	Bottle D
Volume (ml)	10	10	33	33
Initial Activity (mCi)	2	2	2	2
Imaging Time (s/image)	5	10	10	30
Preset $T_{1/2}$ (s)	60	120	120	300

5.3.1 Results

It was soon found that problems were present in the first set of experiments with this configuration. Visually, it was obvious that the water was not mixing well with the activity in the container as it was seen that high dye concentration areas were present toward the bottom of the container, while lighter areas were seen at the top of the container. Additionally, it was found very difficult to maintain a constant flow rate of water into the container using the flowmeters. The inflow rate had to be constantly monitored and adjusted which led to great inaccuracies in the measurement of the washout parameters. Table 5.2 depicts the disappointing results obtained using this experimental setup.

Table 5.2: Results obtained using gravity flowmeters.

	Bottle A	Bottle B	Bottle C	Bottle D
Preset $T_{1/2}$ (s)	60	120	120	300
Actual $T_{1/2}$ (s)	59	103	182	450
Percent Error	1%	14%	52%	50%

It can be seen that this configuration yields very inconsistent results. It seems that the smaller containers give more acceptable results, while the larger containers do not. We attributed this to the fact that mixing was worse in the larger containers and in fact, we could actually see the activity remaining unmixed in the bottom of the larger containers.

5.4 Trial 2: Mixing Holes

It was thought that the incomplete mixing problem could be solved by using a different inlet pipe geometry consisting of many small inlet holes rather than one single large hole. The rationale behind this was that if the inflowing water entered into the container from many places instead of just a single place, then the resultant mixing would take place over a larger volume in the container and hence be more complete. To test this hypothesis, two different experimental configurations were performed. One configuration involved burning a series of many small pinholes into the neoprene tubing while the other involved cutting several larger holes in the side of the tubing. In both configurations, the end of the neoprene tubing was sealed off in order to force the incoming water to move out only through the newly cut holes. Again, flowmeters were used to control the incoming water flow rate.

Experiments performed with this configuration were similar to those attempted in Trial 1, with the exception that data was acquired using a Siemens MultiSPECT 3 triple head camera. Again, only one head was used for data acquisition, and data was stored in a 64x64 matrix with times per frame ranging from 5 - 10 s per frame as summarized in Table 5.3.

Table 5.3: Experiments performed using gravity flowmeters and many inlet holes.

	Bottle A	Bottle B	Bottle C	Bottle D
Volume (ml)	10	10	17	17
Geometry	Pinholes	Scissor holes	Pinholes	Scissor holes
Initial Activity (mCi)	2	2	2	2
Imaging Time (s/image)	5	5	10	10
Set $T_{1/2}$ (s)	60	60	120	120

5.4.1 Results

While the results from these experiments were better than from the previous trial, the containers still suffered from insufficient mixing (see Table 5.4). Now the problem was most pronounced in smaller (10 ml) containers which led us to believe that the real problem was caused by the flowmeters.

Table 5.4: Results obtained using gravity flowmeters and many holes.

	Bottle A	Bottle B	Bottle C	Bottle D
Set $T_{1/2}$ (s)	60	60	120	120
Actual $T_{1/2}$ (s)	83	78	133	120
Percent Error	38%	30%	11%	$< 1\%$

While the smaller holes did indeed lead to better mixing and more consistent results, the washout half-lives still did not meet the 10% accuracy value needed to proceed to phase II. This inaccuracy was attributed to an error in the flowmeters that was greater than stated by the manufacturer. Also, it was found to be very difficult to set the flowmeters at one particular flow rate and to maintain this flow rate over the acquisition time of the experiment. This effect was predominant in the smaller containers and when the inflowing water was set at a very fast rate. Additionally, the flowmeters would have to be constantly monitored and adjusted during the course of the experiment. This would not be an acceptable method of operation once more dynamic containers were used since the demand on the experimenter would be too great.

5.5 Trial 3: Syringe Pump

At this time, a syringe infusion pump became available for our use. This pump consists of a small plunger unit into which a conventional hypodermic needle is placed. The speed

of delivery of the material contained within the syringe is controlled electronically. The error in this pump was stated by the manufacturer to be $< 1\%$ thus giving us very fine control over our inflow rate which should lead to better reproducible results.

For this set of experiments, again the Siemens MS3 camera was used with a 64x64 acquisition matrix. Washout times were preset at either 2 minutes or 4 minutes, and so acquisition times ranged from 5 - 10 s per frame. Again, 2 mCi was used as the initial activity for each container (see Table 5.5).

Table 5.5: Experiments performed using syringe pump and many holes.

	Bottle A	Bottle B	Bottle C	Bottle D
Volume (ml)	17	17	33	33
Initial Activity (mCi)	2	2	2	2
Imaging Time (s/image)	5	10	10	10
Set $T_{1/2}$ (s)	120	120	240	240

5.5.1 Results

This method was tested on the phantom with the pinholes and the results are compiled in Table 5.6. As can be seen, the results are quite encouraging compared to those obtained previously. However, when one draws an ROI on the lower half of the bottle and compares that to an ROI drawn on the upper half of the bottle, a large difference is seen in the washout rates present, Figure 5.2, even though the average of these two washout rates gives the desired washout halftime. Clearly, there is still a problem with the mixing within the container.

Table 5.6: Results obtained using syringe pump and many holes.

	Bottle A	Bottle B	Bottle C	Bottle D
Set $T_{1/2}$ (s)	120	120	240	240
Lower $T_{1/2}$ (s)	97	98	211	202
Upper $T_{1/2}$ (s)	157	141	267	250
Average $T_{1/2}$ (s)	107	107	220	221
Average % Error	11%	11%	8%	8%
Maximum % Error	30%	19%	12%	8%

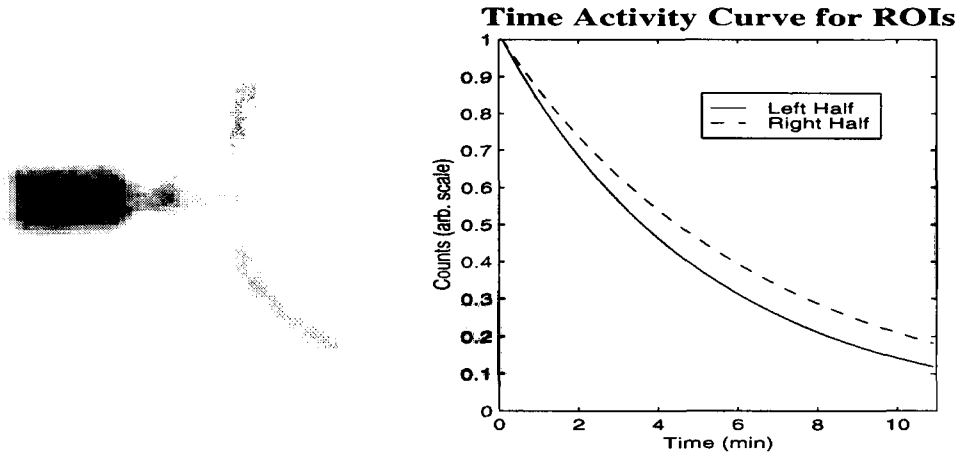

Figure 5.2: Problems seen using the infusion pump and an inlet tube with many holes.

Following this last experiment, it was decided that the best method to ensure thorough mixing within the volume would be to use a mixing propeller placed inside the container. While a propeller could easily be placed inside each container, the question was how to rotate such a propeller as no electrical equipment can be operated in the immediate vicinity of the camera due to interference with sensitive electronics of the camera head.

5.6 Trial 4: Mixing Propellers

The design of the phantom at this point changed drastically as we would have to include a mixing propeller into each of the defect containers. A prototype containing a mixing propeller was designed and built. A long flexible driveshaft that could be attached to the propeller shaft at one end and attached to a small electric motor at the other end was used to rotate the propeller. The length of driveshaft was about 180 cm. This placed the motor at the opposite end of the patient bed and so it allowed both the motor and container to remain far apart and yet move together with the patient bed into the field of view of the camera. Such a configuration is depicted in Figure 5.3.

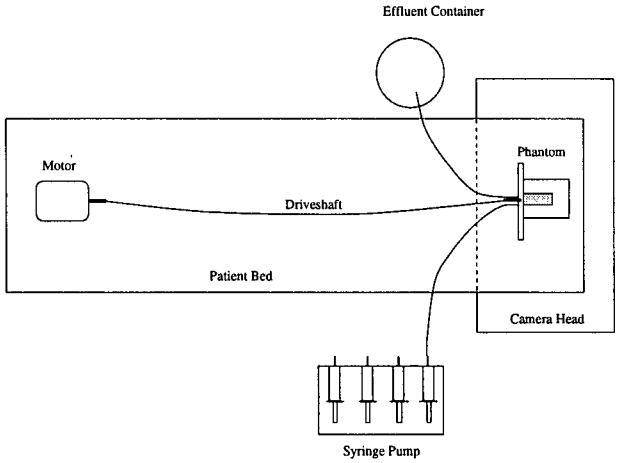

Figure 5.3: Top view of the experimental configuration used for Trial 4. The electrical motor, syringe pump and phantom chamber are shown.

It was decided that the speed of rotation of the motor should not be too high and that a motor capable of several hundred revolutions per minute would be ideal. The motor that was initially tried was a relatively slow 120 revolution per minute 120V AC motor. However, as this motor was uncooled, after the first few experiments, the motor burned out and a substitute had to be found. The replacement motor was a sturdier, fan cooled 120V AC motor that rotated at 600 RPM. While the speed of this motor was a little high,

it was thought that this would be the best solution as slower motors are typically geared down to their lower speeds, and so the electrical load on these types of motors are much higher, leading to a reduced life span.

Data was once again acquired using a similar configuration to that used previously (64x64 matrix, 2 mCi) as shown in Table 5.7.

Table 5.7: Experiments performed using syringe pump and mixing propeller.

	Bottle A	Bottle B	Bottle C	Bottle D
Volume (ml)	17	17	30	30
Initial Activity (mCi)	2	2	2	2
Imaging Time (s/image)	10	10	10	10
Set $T_{1/2}$ (s)	240	240	216	216

5.6.1 Results

In planar tests with this configuration, the experimental halflife agreed very well with that preset on the pump. Additionally, when ROI's were drawn for smaller regions of the container, it was found that they all had very similar washout halflives, thus confirming correct mixing within the container (see Figure 5.4). Table 5.8 depicts the results obtained from this configuration.

Satisfied with consistently good results obtained in planar acquistion mode, we decided to proceed on to phase II, the SPECT trials.

Before proceeding however, since we had a new design for the defect containers that included a mixing propeller, a new design for the myocardial phantom would have to be developed. The final design of the phantom is discussed in the next section.

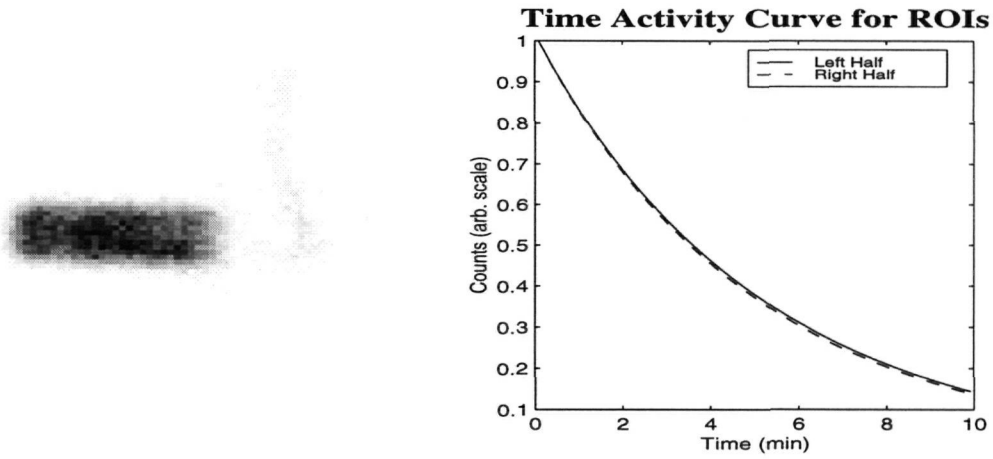

Figure 5.4: Correct mixing attained as shown by matching ROI's on both sides of the container.

5.7 Final Design

The new design of the myocardial phantom consists of five volumes in total, one large volume containing three smaller "defect" inserts and a central blood pool chamber. The smaller containers are arranged in the larger container in a symmetrical manner as shown in Figure 5.5. Different volume "defect" containers can be used consisting as 4 ml, 8 ml, or 17 ml. The larger blood pool volume is a constant 32 ml while the heart volume is dependent upon the number and size of the other containers, and so varies in size from 377 ml to 460 ml.

In order for the equation for dilution to be correct, it is assumed that the mixing of the inflowing water with the liquid in the container is instantaneous. This has been achieved in the phantom by using mixing propellers within each container all attached to a gear system that is driven by a small electric motor. The gear is held atop the mixing unit and is in mesh with a large central gear. This central gear is driven by the electric motor through a flexible drive shaft of length 1.8 m. As mentioned before, this drive shaft is necessary in order for the electric motor to be situated a safe distance from the electronics

Table 5.8: Results obtained using syringe pump and mixing propeller.

	Bottle A	Bottle B	Bottle C	Bottle D
Volume (ml)	17	17	30	30
Initial Activity (mCi)	5	5	5	5
Imaging Time (s/image)	10	10	10	10
Set $T_{1/2}$ (s)	240	240	216	216
Lower $T_{1/2}$ (s)	228	210	193	208
Upper $T_{1/2}$ (s)	244	255	211	218
Average $T_{1/2}$ (s)	231	226	202	211
Average % Error	4%	6%	6%	2%
Maximum % Error	5%	12%	11%	4%

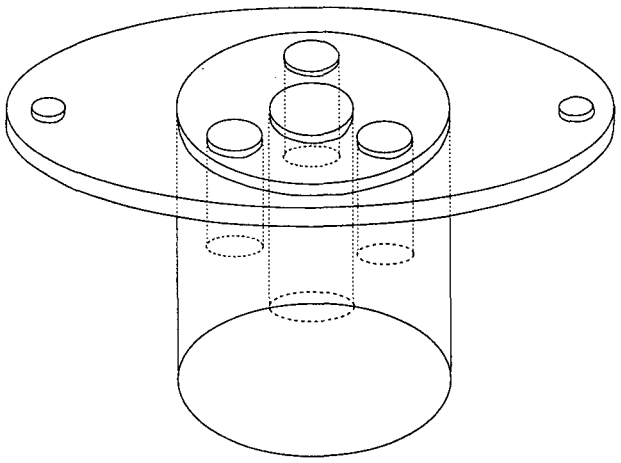

Figure 5.5: The heart phantom used in dynamic SPECT.

in the SPECT camera. The NaI crystal and photomultipliers in the camera head are very sensitive to any electrical fields and so must be kept far away from any electrical activity.

Key to the design of the heart phantom is the mixing units which have to be impermeable to the radioactive water contained within each volume. The design of these mixing units is shown in Figure 5.6. It consists of a plastic apparatus that is held by the top of the heart phantom. Holes are drilled in the lid of the heart to allow the mixing unit to form the tops of the mixing containers. A hole is drilled parallel, but off axis,

to the longitudinal axis of the mixing unit. A brass propeller shaft of diameter 1.5 mm goes through the mixing unit and is held in place on the top by a threaded cap, and in the bottom by a bushing. A rubber O-ring seals the rotating propeller to not allow water from the mixing volume to pass through out of the volume. The water inlet for each container is attached to the mixing unit above the container. A small hole drilled horizontally through the mixing unit stops at the propeller hole. This L shaped hole forms the inlet. The outlet consists of a small hole drilled parallel to the propeller shaft and then horizontally out of the mixing unit. At the outside of each inlet and outlet there is a small 90° elbow which serves to rotate the tubing, hence allowing the units to be placed in close proximity.

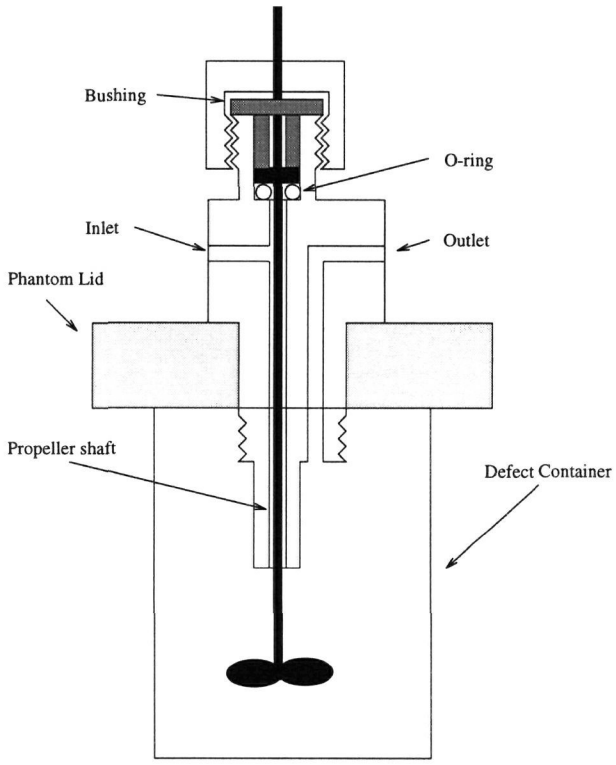

Figure 5.6: A schematic diagram of the mixing units employed in the phantom.

Contained in the heart phantom are a total of seven mixing units. Three of these are

used for the defect containers, one unit is for the central blood pool, while the remaining three are arranged throughout the rest of the heart. It was decided that one mixing unit would be sufficient to mix the activity in each of the small containers and also in the blood pool. However, due to the fact that the defect containers are spaced evenly around the heart, the spaces which exist between these containers could lead to a buildup of activity or of pure water. To remedy this, one mixing unit has been placed within each void, for a total of three mixing units for the heart.

This myocardial phantom may be placed inside a larger thorax phantom (see Figure 5.7). This phantom consists of a cylindrical container 30 cm in diameter and 30 cm tall. Two threaded plastic rods are contained near the middle of the cylinder in order to support the heart phantom. Plastic nuts are used on the top and bottom of the myocardial lid in order to secure the heart in place. Plastic material was used for most parts as it has a very similar attenuating coefficient to that of water.

There exists two celluloid lung objects placed symmetrically in the thorax to model lungs. These lungs have an attenuation coefficient close to that of real lung tissue, but are substantially smaller as they have a volume of only one litre each. Additionally, an aluminum spinal column with a diameter of 3 cm is placed in the phantom. The entire thorax may be filled with water in order to provide a realistic attenuating medium.

Because of the interchangeable design of the entire phantom, it can be used in various configurations ranging from only a simple single container with almost no attenuating material, to the most complicated object, a complete five volume heart model with a non-uniform attenuation due to lungs, thorax and spinal column.

When the entire thorax phantom is used in conjuction with the heart phantom, problems arise in sealing the heart from the thorax, as well as in washing out activity from the heart and driving the mixing propellers. In order to remedy this, another mixing unit is placed on the lid of the thorax phantom directly inline with the central driving propeller of

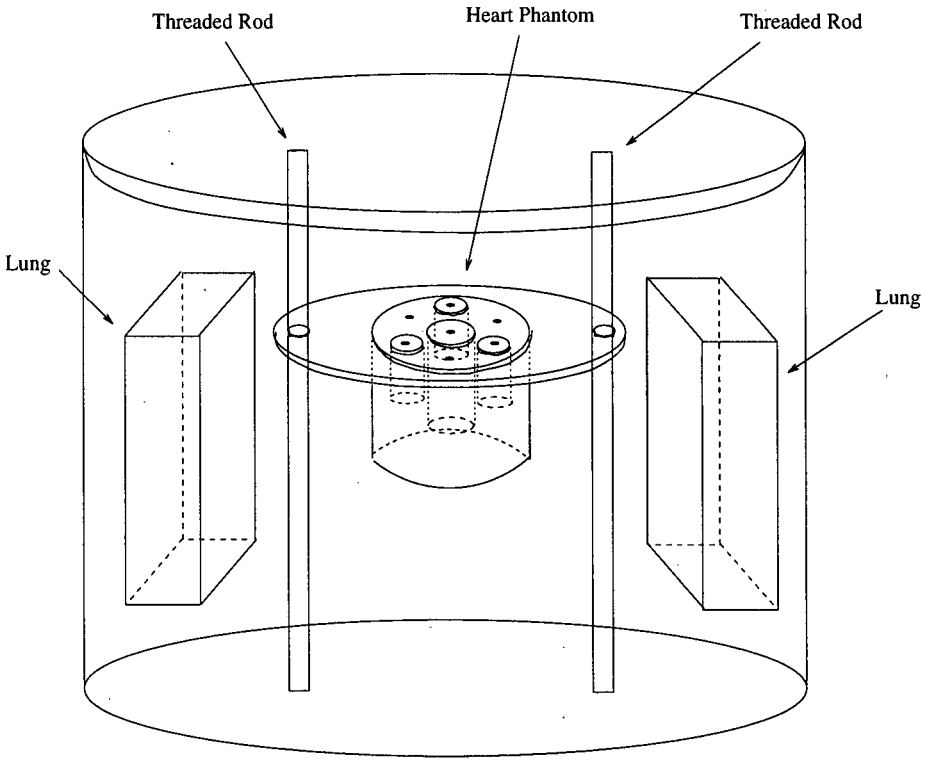

Figure 5.7: A diagram showing the layout of all phantom components.

the heart. A driveshaft is connected from the outer mixing unit to the inner mixing unit. When the outer mixing unit is driven off the electric motor and flexible driveshaft, the inner propeller naturally turns as well, thereby turning the connecting gears and turning all mixing propellers.

In order to wash out the activity, short lengths of neoprene tubing are connected to the inlet and outlet of each mixing unit. At the end of these tubes are snap on connectors that connect with adjoining connectors attached to the thorax lid. When these connectors are not joined, they are sealed, yet when connected, they form a continuous tube, allowing liquids to pass.

Another problem is in the introduction of activity to the containers. Initially the activity was introduced by disconnecting the defect containers from the heart and injecting

activity into them. This procedure works alright when the thorax is not being used, however, when the entire thorax is being used at once, it is inconvenient to empty the large thorax of water and disconnect the entire apparatus in order to insert activity. Therefore, a new design had to be incorporated.

For this new design, it was decided that it would easiest to simply inject activity externally into the defect containers. In addition to providing an easy way of introducing activity into the phantom, it more closely models clinical situations where projection measurements are made prior to the tracer injection in order to determine the input function of the tracer into an organ. In fact, this phantom design allows containers to be connected in series, with water diluting only the first container in the series. This allows for the possibility of modelling a variety of different input functions.

In order to perform this injection, a small length of tubing from an intraveneous drip tube was used. In this section of tubing, there exists a Y-shaped orifice that contains a rubber membrane on one end. The rubber end is made from a natural material that reseals itself when punctured. In an IV drip, this orifice is used for the injection of pharmaceuticals into the patient. Therefore, by using this piece in the exact same way in our phantom, we will have a solution to the problem of activity injection.

5.8 Washout

A single syringe pump used in previous experiments only allows for one syringe to be pumped at a time, thus limiting the number of dynamic containers to only one. Additionally, the maximum syringe volume this pump can hold is 60 ml. When fast washout rates are used, one must be careful not to run out of water in the syringe pump. Consider the example of a 16 ml container with a washout time of 2 minutes, imaged over 20 minutes. During this scan time, the container would require 110.8 ml of water to pass through it,

well beyond the capability of this single syringe pump. Because of these reasons, a ten syringe infusion pump was chosen for this project.

This type of pump allows for up to ten syringes of various sizes to be filled with water and pumped out at a constant rate. The pump is able to handle syringes from a few μl to 140 ml in volume and pump at rates from 0.008 μl/min to 147 ml/min per syringe. The accuracy of the pump has been tested and was found to be accurate to within .5%. In order to pump multiple syringes at different flow rates concurrently, different diameter syringes are used.

The possibility of using different diameter syringes and the fact that the syringe pump operates at a variety of speeds allows infusion rates into the phantom to range from 0 ml per min to 600 ml per min with a maximum total infusion volume of 600 ml. However, realistically, the phantom will be operated under less extreme conditions with several defect containers being used simultaneously. In such a configuration it would be possible for example to perform an experiment with five containers in total (three 17 ml, one 32 ml and one 377 ml) with washout halflives of 1 min, 2 min and 5 min respectively.

5.9 Phase II: SPECT Trials

As mentioned, the next phase in the phantom tests was to try to image the dynamic phantom with a SPECT protocol. This involved an experimental setup very similar to that used in the planar studies, but with different reconstruction and analysis techniques. The method of reconstruction chosen to verify the three dimensional performance of the myocardial phantom was the image based method (IB). The acquisition protocol used is described herein.

In the image based method of dynamic SPECT reconstruction, one requires many reconstructed transaxial images of the same object taken at different times. Ideally, this

would be performed using many sequential rotations of a multiple head SPECT camera. In order to minimize reconstruction artifacts, it is important in IB dynamic SPECT that the rotation time of the camera be fast compared to the washout time of the tracer. The cameras most capable of such an acquistion method are triple head slip ring cameras as these cameras allow continuous rotation in one direction very quickly.

The Department of Nuclear Medicine at Vancouver General Hospital houses a Siemens MultiSPECT 3 (MS3) triple headed SPECT camera. This camera is not a slip ring unit, but is rather capable of only rotating through 360^o before having to reverse directions. Additionally, it was decided that a very fast rotation was not practical as this would lead to poor photon statistics. Therefore, it was chosen to rotate the camera 360^o over 2 minutes.

In order to make the best use of the data acquired over 360^o, a new IB data acquisition and reconstruction protocol was devised. This data acquisition consisted of one 360^o rotation followed by a -360^o rotation, and then another 360^o rotation with each rotation taking 2 minutes. After each rotation, a 2 minute pause was required in order for the computer to save the data to disk and to reset the camera to rotate in the opposite direction. We have developed a method of reconstructing 6 sequential images from a single 360^o rotation through the use of special data handling and manipulation.

In order to reconstruct an object using filtered backprojection it is necessary that projection data be acquired over a continuous 180^o rotation. With a triple head camera rotating over 60^o, this condition can be achieved when the data acquired is properly rearranged. The data acquired over the projection angles $240^o - 300^o$ actually consists of conjugate view data from angles $60^o - 120^o$. That is, the data from detector 3 is the same as that which would be acquired from $60^o - 120^o$, but seen from the opposite side. Therefore, by reordering the data to be: detector 1, (detector 3)$^{-1}$, detector 2, a continuous 180^o projection data set is obtained (see Figure 5.8).

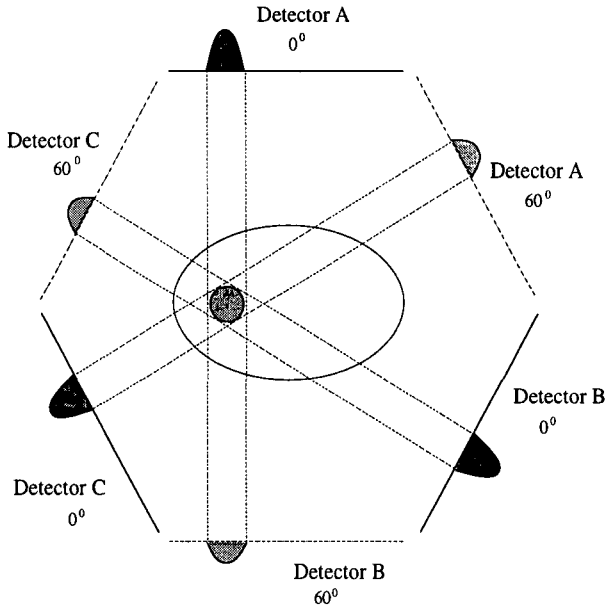

Figure 5.8: Reordering of triple headed camera data over a 60^o rotation in order to achieve a 180^o data set.

Upon continuing the rotation in the same direction for another 60^o, the same reordering procedure can be used to obtain another 180^o continuous data set. However, if reordered the same way as in the first 60^o rotation, projection data covering the range $60^o - 240^o$ will be generated. When reconstructed, the image will appear similar as before, but rotated by 60^o. Upon each succeeding 60^o rotation and reordering, each reconstructed image will be rotated by 60^o relative to the previous image. This effect needs to be corrected for by other data handling procedures.

Once all the projection data has been acquired and aligned, image reconstruction and data analysis can take place. Projection data was reconstructed using the Maximum Likelihood - Ordered Subsets (ML-OS) algorithm into a series of 18 transaxial images. Once reconstructed, the data is analyzed by drawing ROI's on each image and plotting the number of counts in each ROI vs the time in a manner similar to that used for dynamic planar studies. The result of such an analysis yields a time activity curve for

the transaxial region. The TA curves were then analyzed by fitting a single exponential function to this data and determining the parameters of the best fit. These experimental washout parameters can then be compared to those set on the pump in order to verify the phantom performance in three dimensions.

Another method to verify the phantom performance combines both SPECT acquisition with planar techniques. If the object under study is not placed in the exact center of rotation of the camera, as the camera rotates, it will be seen to move within the field of view as in Figure 5.9, therefore, one cannot analyze dynamic projection data in the same way as planar data (ie, draw a ROI and create a TA curve). However, a method very similar to planar dynamic analysis can be used if only one object is studied.

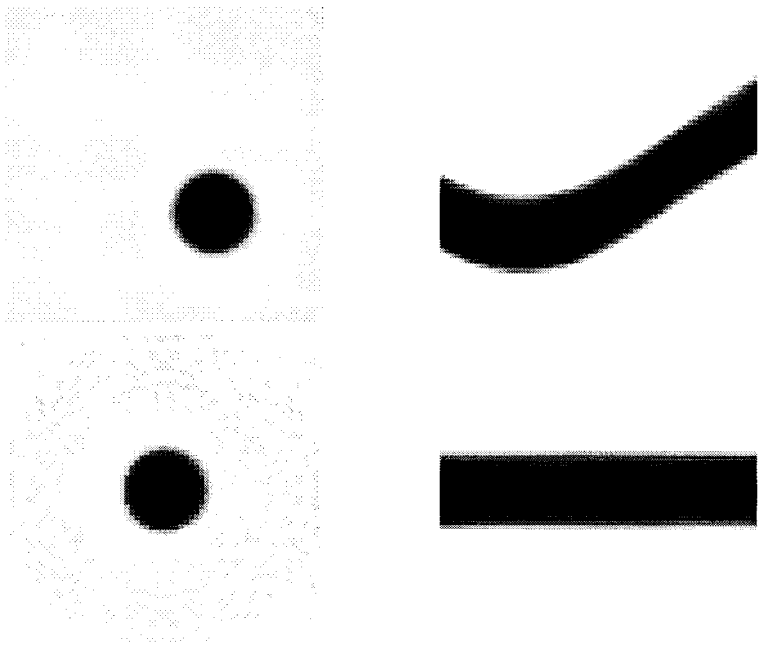

Figure 5.9: Motion of an offset object on the camera as seen from various projections (top) compared the motion of an object centered in the field of view (bottom).

If we plot the total counts for each projection vs the time each projection was taken, we end up with a time activity curve (see figure 5.10. By fitting this TA curve with a

monoexponential function, we can determine the actual washout time of the bottle as in a dynamic planar study, but by using a SPECT acquisition protocol. Results for the phantom in both IB SPECT and projection mode are shown in Table 5.9.

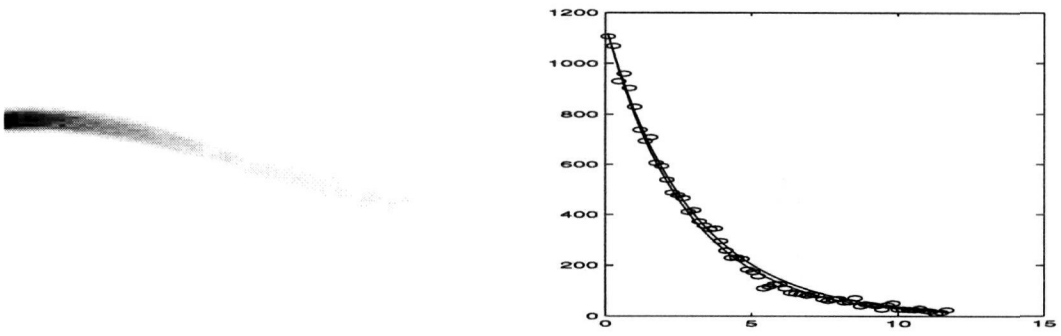

Figure 5.10: Dynamic SPECT projection data for a single slice analyzed by time activity curve analysis. ROI's are drawn over each projection measurement (in this case, over each vertical line).

Table 5.9: Experimental SPECT results obtained with phantom.

IB SPECT Results

	Bottle A	Bottle B	Bottle C	Bottle D
Volume (ml)	17	17	32	32
Preset $T_{1/2}$ (s)	240	240	216	216
Projection $T_{1/2}$ (s)	233	246	230	224
SPECT $T_{1/2}$ (s)	217	222	223	208
Percent Error	7%	10%	3%	7%

CHAPTER 6

DYNAMIC SIMULATIONS

As a preliminary excursion into developing dynamic SPECT reconstruction algorithms, some computer simulations have been performed. Computer simulations are useful in order to refine data acquisition procedures prior to performing any costly experiments.

Dynamic SPECT projection data has been simulated for a variety of configurations for single, dual and triple headed cameras. The purpose of these simulations was to determine optimal acquistion protocols and to create data for initial testing of dynamic SPECT reconstruction algorithms. A variety of geometrical configurations were used with different washout rates and acquisition protocols.

6.1 ANALYTICAL SIMULATIONS

The simplest analytical object to simulate is a circle of uniform activity. For such an object, a two dimensional function representing the object is created. For the circle offset from the origin by an amount (a,b), we have,

$$(x-a)^2 + (y-b)^2 = r^2 \tag{6.1}$$

As the camera rotates, the apparent position of this object will appear to change relative the original axes. For a rotation of θ degrees, the new axes become,

$$x\prime = xcos\theta + ysin\theta \quad and \quad y\prime = -xsin\theta + ycos\theta \tag{6.2}$$

The object at the new point $(x\prime, y\prime)$ is then defined using equation 6.1. Projections of this object can be determined by performing line integrals at this new postion. That is, the projection value at the position $x\prime$ at angle θ is given as the line integral of the function at this new point. In the case of the circle, the line integral is simply equal to twice the $y\prime$ value. Therefore, in equation 6.1, the x and y are replaced with $x\prime$ and $y\prime$ and solved for $y\prime$ to yield the value of the line intergral. Solving 6.1 for $y\prime$ gives us,

$$y\prime = \sqrt{r^2 - (x\prime - a)^2} + b \tag{6.3}$$

and a continuous function in $x\prime$ is obtained. This function must be discretized into camera bins in order to be reconstructed using conventional methods. To discretize the data, it has been chosen to solve for $y\prime$ only at the locations in $x\prime$ corresponding to the mid points of the camera bins. Therefore, in the case of 64 bins, $x\prime$ normally runs from -32,-31,...,-1,1,...,31,32. In order to bin the line integrals, the line integrals only at the points -31.5,-30.5,...,-.5,.5,...,30.5, 31.5 were evaluated.

After the projection is produced, the camera bin values must be adjusted to match the amount of activity present. This is done by multiplying the projection data by a constant that is proportional to the initial activity present and the acquisition time taken for each projection. This then represents the actual number of counts detected in the camera over a projection time t.

In order to simulate dynamic data, washout of the activity must occur as the camera rotates around the object. This is done by multiplying each projection measurement by

a decay factor. In our initial simulations, a single exponential function was used. Thus, each projection was adjusted so as to give a revised activity of,

$$y\prime(x\prime,t) = [\sqrt{r^2-(x\prime-a)^2}+b]\cdot exp(-\lambda t) \tag{6.4}$$

Alternatively to using line integrals to evaluate the projections, area integrals can be used. The function is defined in the rotated axes as above, but this time, an integration of $y\prime$ is performed over the width of each bin. That is the integral in the ith bin of the kth projection angle is,

$$C = \int_{x'-.5}^{x'+.5} y'dy' \tag{6.5}$$

By performing the projection in this way, no approximation is made that the value over the entire bin is represented by the integral over only the middle point of the bin as was made in the line integral method. As well, the value in each bin is already discretized to the exact area of the projection. The data still needs to be scaled depending upon the total number of counts and the acquisition time as in the line integral method. Dynamic decay is also simulated in the same way by simply scaling down succeeding projections by a function representing an exponential decay.

6.2 Pixelized Simulations

In order to perform pixelized simulations, we must be able to determine the projections of pixelized objects. The method used involves computing a system weighting matrix that creates projections based upon the equation,

$$D = Sx \tag{6.6}$$

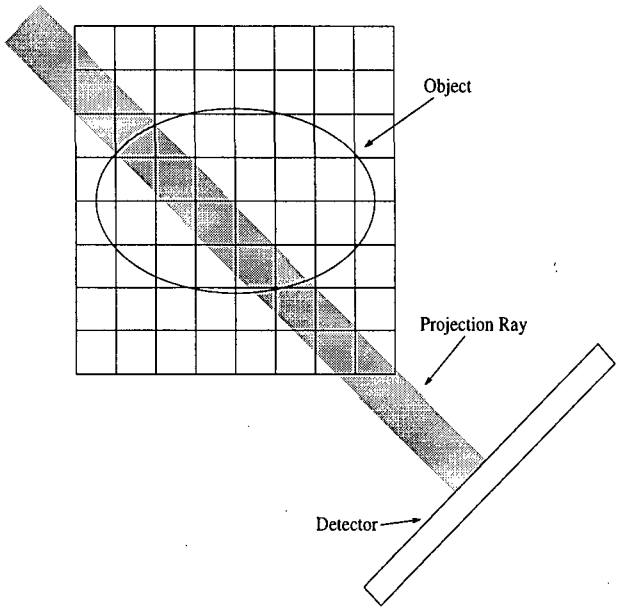

Figure 6.1: The meaning of the system weighting matrix S. Each value in S represents the area of a pixel intersected by a projection line.

where D is the vector representing the projection data, S is the system weighting matrix and x is the vector representing the object data. Each element of S corresponds to the area of pixel-ray intersection and can be computed analytically. The exact meaning of the S matrix can be seen in Figure 6.1

This S matrix can be used to create projection data and also to reconstruct the image from the projection data by taking S^{-1}. Due to it's large size and the sparcity, the inversion of this matrix is not a trivial task and techniques have been proposed which attempt to find its inverse.

In dynamic simulations, the object data matrix x consists of many time dependent functions. As an example, consider the case of myocardial metabolism of fatty acids as explained in Chapter 3. In such a case, the pixel activity at any time, t_k can be described by the dual exponential function,

$$x_i(t_k) = A_i e^{-\lambda_i t_k} + B_i e^{-\gamma_i t_k} + C_i \tag{6.7}$$

where λ_i and γ_i are decay parameters for the ith pixel. If attenuation is taken into account as well, each x_i will be additionally decreased as,

$$x_i(t_k)' = x_i(t_k) e^{-\mu_{jk} l_{jk}} \tag{6.8}$$

where μ is the attenuation coefficient for the ith pixel and l is the projection ray length for the kth projection.

In most simulations performed to date, no attenuation was taken into account as in order to test the reconstruction methods, as simple a model as possible should be used. To aid in simplicity, perfect parallel hole collimators were used and washout was assumed to follow a single exponential function as was tested with the phantom.

6.2.1 IB Simulations Performed

A number of different simulations involving various objects were performed using the IB acquisition protocol as described in Chapter 5. Variables included the time per rotation, t_acq, the amount of activity present and the washout time of the tracer, $T_{1/2}$. A useful parameter introduced at this point is the variable Γ. This variable corresponds to,

$$\Gamma = \frac{T_{1/2}}{t_{acq}} \tag{6.9}$$

As well, different simulations were performed with different numbers and shapes of objects. Table 6.1 summarizes the simulations performed.

Table 6.1: IB simulations performed

Geometry	Rotation Time Minutes	Washout Time Minutes	Γ	Activity mCi
Single circle	2+2+2 (w/pause)	2	6	.1
Single circle	2+2+2 (w/pause)	5	15	.1
Four circles	2+2+2 (w/pause)	2,4,6,10	6,12,18,30	.1
Four circles	5+5+5 (w/pause)	2,4,6,10	2.4, 4.8, 7.2, 12	.1
Annulus	2+2+2 (w/pause)	2,4,6,10	6, 12,18,30	.1
Annulus	5+5+5 (w/pause)	2,4,6,10	2.4, 4.8, 7.2, 12	.1
Annulus (w/noise)	2+2+2 (w/pause)	2,4,6,10	6,12,18,30	.1

6.3 Direct Parameter Simulations

The other simulation acquistion protocol is for the reconstruction method known as the direct parameter method. This method uses a much simpler data acquistion protocol as the reconstruction method was designed for a single headed camera rotating over 180^o.

6.3.1 DP Simulations Performed

Similar experiments were performed with using the DP acquisition protocol. These simulations are summarized in Table 6.2.

Table 6.2: DP simulations performed

Geometry	Rotation Time Minutes	Washout Time Minutes	Γ	Activity mCi
Single circle	10	2	.2	.1
Single circle	10	5	.5	.1
Four circles	10	2,4,6,10	.2,.4,.6,1	.1
Four circles	20	2,4,6,10	.1,.2,.33, .5	.1
Segmented Annulus	10	2,4,6,10	.2,.4,.6,1	.1
Segmented Annulus	20	2,4,6,10	.1,.2,.33,.5	.1
Segmented Annulus (w/noise)	10	2,4,6,10	.2,.4,.6,1	.1

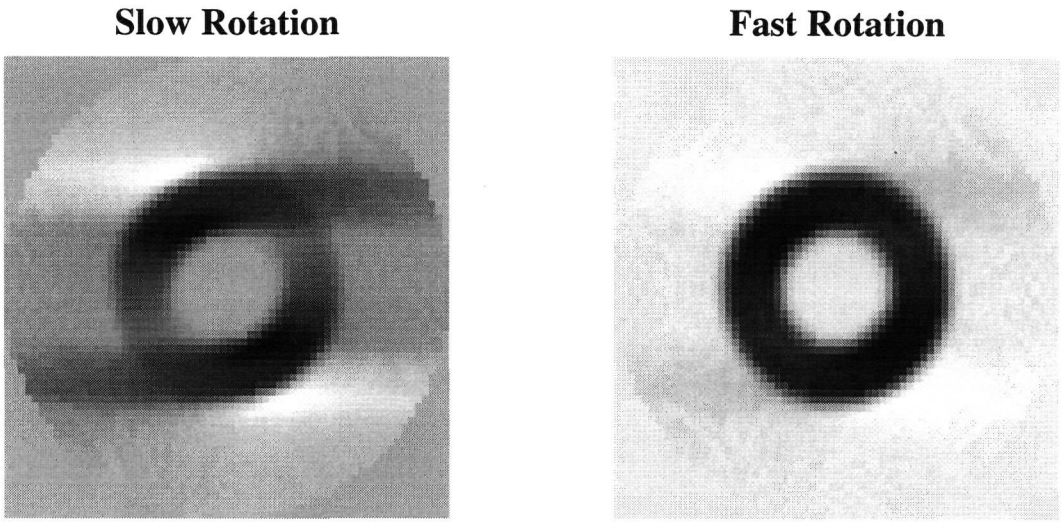

Figure 6.2: Typical results obtained for the image based reconstruction method.

6.4 IB Simulation Results

When dynamic SPECT data is reconstructed using a conventional SPECT reconstruction technique (eg, filtered backprojection, ML-OS, etc), severe artifacts result. This is due to the fact that these algorithms assume a stationary distribution of activity over time.

If the speed of rotation is relatively fast compared to washout times involved, the streaking artifact will be minimized. This is the principle of the image based method. As can be seen in Figure 6.2, if the rotation speed is fast, almost no artifact is present. This results in a good differentiation in the image and so a clear TA curve can be drawn. When the TA curve is analyzed, it yields a smooth exponential function.

It has been found through these simulations that the IB method of dynamic SPECT performs well providing that the rotation time of the camera is relatively fast compared to the washout time of the tracer. Quantitatively, the speed of rotation should be at least twice the biological half-life of the tracer in order to minimize the steaking artifact. This means that for $\Gamma > 2$, the streaking artifact will be minimal, agreeing with [21].

Our proposed acquisition method for the IB protocol meets this criteria for a 2 minute rotation as each image will represent only a 20 second movement of tracer. As well, a five minute rotation could also be sufficient to image most biological processes using the IB protocol as this would correspond to an acquistion time of 50 seconds.

However, it has also been found that even with a five minute rotation, the number of counts detected by the camera may not be enough in order to reconstruct useful images, particularly at later imaging times. This is explained by using the following example of myocardial viability.

A typical clinical myocardial viability study involves the injection of 5-10 mCi of activity into the patient. This amount corresponds to a count rate of about $1.85 - 3.7x10^7$ counts per second (cps). Taking into account the camera efficiency (.01 %) and averaging over 64 slices, this gives an average count rate per slice of only 300 - 600 cps. Because the statistical uncertainty associated with radioactive decay is Poisson, then the error in the number of counts can be approximated as $\sqrt{C}$. For the count rate of 300 cps, over a projection time of 20 s, the error in the number of counts will be about 2 %.

This error is when the tracer is at its highest concentration however, and since the tracer washes out with an exponential decay, the count rate will continuously be diminished, thereby increasing the relative error. In the noiseless simulations this effect cannot be seen, but when noise is added to the projection data, this effect becomes noticeable (see Figure 6.3).

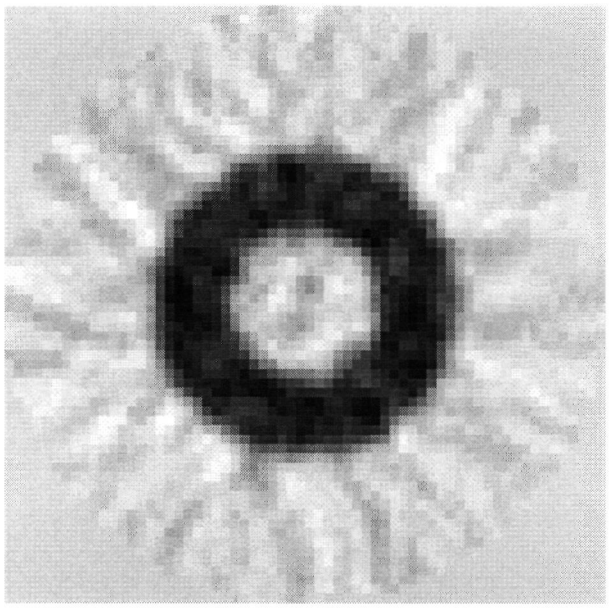

Figure 6.3: The effect of noise on reconstructed dynamic image quality.

6.5 DP Simulation Results

Simulations performed using the DP acquisition protocol were reconstructed using several reconstruction algorithms. One DP technique uses *a priori* information regarding the washout of tracer. In this method it is assumed that the washout of tracer follows a dual exponential function as described previously. Therefore, one can attempt to determine the washout parameters associated with this washout by attemping to minimize the non-linear least squares (NLS) equation,

$$min \left\{ \sum_{j,k} \sigma_{jk}^{-2} \left(\sum_{i} a_{ijk} x_i(t_k) - d_{jk} \right)^2 \right\} \tag{6.10}$$

where,

$$x_i(t_k) = A_i e^{-\lambda_i t_k} + B_i e^{-\eta_i t_k} + C_i \tag{6.11}$$

Results obtained using the NLS technique are able to reconstruct washout times to

within 20% accuracy, but are computationally intensive and not practical clinically.

Another method that uses a linear least squares again solves equation 6.10, but this time replacing $x_i(t_k)$ with the constraint that the activity contained within each pixel at each projection time is less than or equal to the activity at the previous time [38]. That is,

$$x_i(t_1) \geq x_i(t_2) \geq ... \geq x_i(t_{n-1}) \geq x_i(t_n). \tag{6.12}$$

Preliminary results of the LLS algorithm are able to reconstruct washout times to about 50% accuracy with a substantial time savings over the NLS method. New methods are being developed that should be able to reconstruct washout times with improved accuracy [39, 40, 41].

CHAPTER 7

CONCLUSION

Nuclear medicine imaging is inherently a functional imaging modality which allows one to observe the inner function of specific organs and the metabolism of specific compounds. This ability enables physicians to make better diagnosis when the anatomy of an organ is not in question, but rather when its function requires investigation.

As physiological rates are functions of time, the values of the related kinetic parameters are useful measures of the organs functional ability. Rather than solely relying on the fact that radiophamaceutical uptake takes place, we are more concerned with the speed of the compound uptake, metabolism and extraction. These types of dynamic studies are commonly performed in nuclear medicine with planar techniques or PET, but it is hoped that new techniques being developed will use common SPECT cameras in order to obtain this information in three dimensions.

7.1 REVIEW OF THIS WORK

We have designed and built a dynamic myocardial heart-in-thorax phantom for use in nuclear medicine dynamic imaging. The principle of the phantom is based on a model of fatty acid metabolism within the myocardium in which the washout of tracer from

the myocardium can be described by a dual exponential function in time. We are able to model such a dual exponential functional by diluting activity in a volume with water using the techniques described in Chapter 4.

Through testing the phantom first in planar mode, we have determined that the final design is capable of being used in the development of new dynamic SPECT methods. It's been found that the phantom is able to reproduce preset washout rates to within 10% accuracy. This means that we can now preset the phantom to a specific washout rate, and be certain that the tracer washout actually corresponds to this.

Preliminary results using the phantom with the IB acquisition protocol show that we are able to reconstruct SPECT washout times to within 10% of the preset values. This has been verified through the analysis of projection data.

7.2 Other Phantom Applications

The phantom that has been described in this work was designed for fatty acid myocardial studies. However, due to the flexible design of the phantom, it lends itself well to the study other regions within the body.

Renal studies may be performed using the same phantom with the central blood pool container removed. This will provide an organ of maximum volume and the correct general shape for a kidney. When used as a kidney, the phantom would be measuring extraction fractions or renal blood flow. Again, the phantom would be injected with some radiotracer and allowed to wash out the tracer through the infusion of pure water. Time activity curves could then be drawn and fit with the appropriate model, probably a non-compartment model described in Chapter 3.

Dynamic heptabiliary studies could be performed in a similar manner to the renal studies by using the phantom in the same configuration. As described in Chapter 3, in

most non-compartmental studies, the input function used is an ROI drawn over the left ventricle. It would be possible to develop an entire dynamic thorax phantom that contains a dynamic heart, dynamic liver, and dynamic kidneys all working together to provide a realistic dynamic model. Such a phantom would use the same principles used in the heart developed, but include three other containers for the liver and kidneys. The input into the liver and kidneys would come straight from the output of the heart, thus providing the input funtions described.

Another application of the phantom is in the assessment of regional cerebral blood flow. With such an application, it would perhaps be better to use a brain shaped phantom, but all the inner parts could be identical to the myocardial phantom.

7.3 Final Word

The design of the dynamic myocardial phantom has been to create a phantom that models various dynamic processes in the body. This design goal has been met as the phantom is capable of a wide range of different dynamic models ranging from single exponential washout, multiple exponential washout, and even modelling input functions.

Because of the wide range of applications available to the phantom, it will play a key role in the development of new dynamic imaging algorithms. In this work, the application of the phantom to dynamic SPECT has been concentrated upon, but other dynamic imaging modalities such as PET or MRI may also potentially benefit from the phantom.

BIBLIOGRAPHY

[1] S. Nellis, A. Liedtke, and B. Renstrom. Fatty acid kinetics in aerobic myocardium:Characteristics of tracer carbon entry and washout and influence of metabolic demand. *J. Nuc. Med.*, 33:1864–1874, 1992.

[2] M.P.J. Hudon, D.M. Lyster, W.R.E. Jamieson, A.K. Qayumi, C. Sartori, and H.A. Dougan. The metabolism of (^{123}I)-iodophenyl pentadecanoic acid in a surgically induced canine model of regional ischemia. *Eur. J. Nuc. Med.*, 16:199–204, 1990.

[3] G. Hounsfield. Computerized transverse axial scanning (tomography): Part I. Description of system. *Brit. J. Rad.*, 47:1016–1022, 1973.

[4] P. Lauterbur. Image formation by induced local interactions: Examples employing nuclear magnetic resonance. *Nature*, 242:190–191, 1973.

[5] J.A. Sorenson and M.E. Phelps. *Physics in Nuclear Medicine.* W.B. Sauders Company, 1987.

[6] H.O. Anger. Scintilation camera with multichannel collimators. *J. Nuc. Med.*, 5:515–531, 1964.

[7] M.E. Phelps, J.C. Mazziotta, and H. Schelbert, editors. *Positron Emission Tomography and Autoradiography: Principles and Applications in Brain and Heart.* Raven Press, New York, 1986.

[8] L.A. Shepp and Y. Vardi. Maximum liklihood reconstruction for emission tomography. *IEEE Trans. Med. Imag.*, MI-1:113–122, 1982.

[9] X. Xiao-Liang, L. Jeih-San, and S.C. Strother. Iterative algebraic reconstruction algorithms for emission computed tomography: A unified framework and its application to positron emission tomography. *Med. Phys.*, 20:1675–1684, 1993.

[10] S.R. Deans. *The Radon transform and some of its applications.* John Wiley & Sons, Toronto, 1983.

[11] G. Liu, G. Soberling, J. Duyn, and C. Moonen. A functional MRI technique combineing prionciples of echo-shifting with a train of observables (PRESTO). *Mag. Res. Med.*, 30:764–768, 1993.

[12] U. Buschsieweke, C. Promper, J. Smolorz, and H. Kutzim. Functional analysis of magnetic resonance studies of the heart. *Diagn. Imag. Clin. Med*, 55:72–76, 1986.

[13] P. Bandettini, A. Jesmanowicz, E. Wong, and J. Hyde. Processing strategies for time-course data sets in functional MRI of the human brain. *Mag. Res. Med.*, 30:161–173, 1993.

[14] A. Kato, D. Menon, M. Diksic, and Y. Yamamoto. Influence of the input function on the calculation of the local cerebral metabolic rate for glucose in the deoxyglucose method. *J. Cereb. Blood Flow Metab.*, 4:41–46, 1984.

[15] W. Heiss, G. Pawlik, K. Herholz, R. Wagner, H. Goldner, and K. Wienhard. Regional kinetic constants and cerebral metabolic rate for glucose in normal human volunteers determined by dynamic positron emission tomography of 18F-2-Fluoro-2-deoxy-D-glucose. *J. Cereb. Blood Flow Metab.*, 4:212–223, 1984.

[16] E. Tsui and T. Budinger. Transverse section imaging of mean clearance time. *Phys. Med. Biol.*, 23:644–653, 1978.

[17] R.E. Carson, S.C. Huang, and M.V. Green. Weighted integration method for local cerebral blood flow measurements with positron emission tomography. *J. Cerebral Blood Flow and Metabolism*, 6:245–258, 1986.

[18] B.M. Mazoyer, R.H. Huesman, T.F. Budinger, and B.L. Knittel. Dynamic PET data analysis. *J. Computer Assisted Tomography*, 10:645–653, 1986.

[19] J. Matthews, D. Bailey, P. Price, and V. Cunningham. The direct calculation of parametric images from dynamic PET data using maximum-likelihood iterative reconstruction. *Phys. Med. Biol.*, 42:1155–1173, 1997.

[20] K. Chen, S. Huang, and D. Feng. New estimation methods that directly use the time accumulated counts in the input function in quantitative dynamic PET studies. *Phys. Med. Biol.*, 39:2073–2090, 1994.

[21] B. Bok, A. Bice, M. Clausen, D. Wong, and H. Wagner. Artifacts in camera based single photon emission tomography due to time activity variation. *Eur. J. Nucl. Med.*, 13:439–442, 1987.

[22] K. Nakajima, N. Shuke, J. Taki, T. Ichihara, N. Motomura, H. Bunko, and K. Hisada. A simulation of dynamic SPECT using radiopharmaceuticals with rapid clearance. *J. Nuc. Med.*, 33:1200–1206, 1992.

[23] M.K. O'Connor and D.S. Cho. Rapid radiotracer washout from the heart: Effect on image quality in SPECT performed with a single-headed gamma camera system. *J. Nuc. Med.*, 33(6):1146–1151, 1992.

[24] R. Stewart, M. Schwaiger, G. Hutchins, P. Chiao, K. Gallagher, N. Nguyen, N. Petry, and W. Rogers. Myocardial clearance kinetics of technetium-99m-SQ30217: A marker of regional myocardial blood flow. *J. Nuc. Med.*, 31(7):1183–1190, 1990.

[25] R. Rowe, H. Barret, J. Chen, J. Hall, W. Klein, B. Moore, I. Pang, D. Patton, and T. White. A stationary 3D SPECT brain imaging system. *J. Nuc. Med.*, 32(15):1135, 1991.

[26] M. Rogulski, H. Barrett, W. Klein, I. Pang, D. Patton, D. Richards, J. Sain, W. Smith, and D. Wilson. FastSPECT: A new dimension to single photon emission computed tomography (SPECT). *J. Nuc. Med.*, 36(5):268P–269P, 1995.

[27] B. Holman, P. Carvalho, R. Zimmerman, K. Johnson, S. Tumeh, A. Smith, and S. Genna. Brain perfusion SPECT using an annular single crystal camera: Initial clinical experience. *J. Nuc. Med.*, 31(9):1456–1461, 1990.

[28] S. Ross, A. Welch, G. Gullberg, and R. Huesman. An investigation into the effect of input function shape and image acquisition interval on estimates of washin for dynamic cardiac SPECT. *Phy. Med. Biol.*, 42:2193–2213, 1997.

[29] A.M. Smith, G.T. Gullberg, P.E. Christian, and F.L. Datz. Kinetic modeling of teboroxime using dynamic SPECT imaging of a canine model. *J. Nuc. Med.*, 35:484–495, 1994.

[30] H. Iida, H. Itoh, M. Nakazawa, J. Hatazawa, H. Nishimura, Y. Onish, and K. Uemura. Quantitative mapping of regional cerebral blood flow using Iodine-123-IMP and SPECT. *J. Nuc. Med*, 35:2019–2030, 1994.

[31] M.P. Hudon, D.M. Lyster, W.R.E. Jamieson, A.K. Qayumi, M. Keiss, L.J. Rosado, A.P. Autor, C. Sartori, H. Dougan, and J. Van Den Broek. Efficacy of (^{123}I)-iodophenyl pentadecanoic acid (IPPA) in assessment myocardial metabolism in a model of reversible global ischemia. *Eur. J. Nuc. Med.*, 14:594–599, 1988.

[32] G. Gullberg, R. Huesman, S. Ross, E. Di Bella, G. Zeng, B. Reutter, P. Christian, and S. Foresti. *Nuclear Cardiology: State of the art and Future Directions*, chapter Dynamic cardiac single photon emission computed tomography. Mosby-Year Book, Inc, Philadelphia, PA, in press.

[33] H. Machulla, M. Marsmann, and K. Dutschka. Biochemical concept and synthesis of a radioiodinated phenylfatty acid for in vivo metabolic studies of the myocardium. *Eur. J. Nuc. Med.*, 5:171–173, 1980.

[34] T. DeGrado, J. Holden, C. Ng, D. Raffel, and S. Gatley. Quantitative analysis of myocardial kinetics of 15-p-[Iodine-125] iodophenylpentadecanoic acid. *J. Nuc. Med.*, 30:1211–1218, 1989.

[35] H. Schelbert. Metabolic imaging to asses myocardial viability. *J. Nuc. Med.*, 35:8S–14S, 1994.

[36] S. Bergmann. Use and limitations of metabolic tracers labeled with poitron-emitting radionuclides in the identification of viable myocardium. *J. Nuc. Med.*, 35(4S):15S–22S, 1994.

[37] A. Celler, T. Farncombe, R. Harrop, and D. Lyster. Dynamic heart-in-thorax phantom for functional SPECT. *IEEE Trans. Nuc. Sci.*, 44(4):1600–1605, 1997.

[38] J.Maeght. Tomographie. problemes de moindres carees. In *Rapport de DEA, Universite P.Sabatier, Toulouse*, August 1997.

[39] H. Wu, C. Hoh, Y. Choi, H. Schelbert, R. Hawkins, M. Phelps, and S. Huang. Factor analysis for extraction of blood time-activity curves in FDG-PET studies. *J. Nuc. Med.*, 36(9):1714–1722, 1995.

[40] A. Houston and W. Sampson. A quantitative comparison of some FADS methods in renal dynamic studies using simulated and phantom data. *Phys. Med. Biol.*, 42:199–217, 1997.

[41] H.H. Bauschke, D. Noll, A. Celler, and J.M. Borwein. An EM-algorithm for dynamic SPECT tomography. *IEEE Trans. Med. Img.*, 1997. Submitted [CECM research report 97-092].